



**Bachelor of Engineering with Honours in
Mechanical Engineering
(Full Time)**

324 MAE Individual Project

**Design of a Bio-inspired Thruster for Remotely
Operated Vehicles**

**Project Supervisor
Dr. Tan Weng Chun Jason**

**Submitted by –
Aung Kyaw Kyaw (14931910)**

**Submission Date
23-02-2025**

**Word Count
7859
(Main Body)**

Abstract

This report explores the design and development of a bio-inspired thruster for Remotely Operated Vehicles (ROVs), focusing on enhancing manoeuvrability and efficiency through biomimicry. Traditional ROV relies on conventional fan propellers for movement. This increases the power consumption and difficult to maintain stable position, especially at harsh underwater conditions. By imitating the propulsion mechanism of marine animals, these limitations are addressed as the project's key problem statements. The methodology includes conceptual design ideas, kinematic and dynamic modelling, material selection, and functional assembly modelling and culminates in the prototype development. The results from simulations and experimental testing validate the bio-inspired thruster's performance, demonstrating improvements in manoeuvrability and efficiency. The discussion further analyses the implications of these findings for ROV technology, with recommendations for future work to enhance the thruster's design and integration into existing ROV frameworks.

Declaration

I hereby declare that this report, titled "Design of a Bio-Inspired Thruster for Remotely Operated Vehicles" is submitted as part of the requirements for the Bachelor of Engineering (Hons) in Mechanical Engineering at Coventry University. The work presented herein is entirely my own, completed between 11/20/2024 and 2/27/2025, under the supervision of Dr. Tan Weng Chun Jason.

I further confirm that this report has not been submitted previously, in whole or in part, for any academic qualification at Coventry University or any other institution.

Aung Kyaw Kyaw

2/21/2025

Name

Date

Acknowledgment

Firstly, I would like to express my deepest gratitude to my parents for their unwavering financial and emotional support, which has allowed me to pursue my studies with confidence.

Secondly, I extend my sincere appreciation to my supervisor, Dr. Jason, for his invaluable guidance and constructive feedback throughout this project. His insights and expertise have been instrumental in refining my research and design approach.

Furthermore, I am also grateful to the professors and lecturers at Coventry University for their teachings, which have contributed to my academic development. I also acknowledge the laboratory engineers for their assistance with hardware and technical support.

Lastly, I appreciate the support of my peers, particularly Min Thant Kyaw and Kaung Khant Oo for their assistance in assembling the prototype, and Aung Myat Thu for providing access to his pool for experimental testing.

Table of Contents

Abstract	i
Declaration	ii
Acknowledgment.....	iii
1. Introduction	1
1.1 Background	1
1.2 Problem Statement and Research Questions	2
1.3 Aim and Objectives	3
1.4 Scope and Limitations	3
1.5 Report Outline	4
1.6 Gantt Chart.....	5
2. Literature Review	6
2.1 Overview of ROVs	6
2.2 Review of Thrusters.....	8
2.2.1 Thruster Configuration.....	10
2.2.2 Manoeuvrability Challenges	11
2.3 Bio-inspired Technology.....	12
2.3.1 Aboveground Bio-inspired Robots	12
2.3.2 Underwater Bio-inspired Robots	13
3. Methodology.....	16
3.1 Flow Chart	16
3.2 Conceptual Designs.....	18
3.2.1 Concept 1 – Cownose Ray-Inspired Linkage Mechanism	18
3.2.2 Concept 2 – Seahorse-Inspired Oscillating Fin Mechanism	19
3.2.3 Concept 3 – Fish Tail-Inspired Cam-Like Mechanism	20
3.2.4 Design Constraints	22
3.2.5 Design Criteria	22
3.2.6 Final Design Selection	23
3.3 Kinematic and Dynamic Modelling.....	24
3.3.1 Fin Shape and Motion	24
3.3.2 Servo Motion	24
3.3.3 Fin Thrust Force	25
3.3.4 Fin Drag Force and Lift Force	25

3.3.5 Servo Energy Consumption	26
3.3.6 Degrees of Freedom	26
3.4 Material Selection	28
3.4.1 Frame Material	28
3.4.2 Thruster Material	28
3.4.3 Electronics Enclosure & Components	29
3.4.4 Buoyant Foams, Ballasts & Miscellaneous Components	30
3.5 Functional Assembly Model	31
3.5.1 2D Drawings.....	31
3.5.2 3D CAD Model	33
3.6 Design Functionality	37
3.6.1 FAST Diagram.....	37
3.6.2 Design for Manufacture and Assembly (DFMA)	38
3.6.3 Failure Mode and Effect Analysis (FMEA).....	41
3.7 Preliminary Analysis of Stress and Hydrodynamic Loads	43
3.7.1 Finite Element Analysis (FEA) Simulation	43
3.7.2 Computational Fluid Dynamics (CFD) Simulation	45
3.8 Prototyping	46
3.8.1 Process of Fabrication	46
3.8.2 Final Assembly	51
3.8.3 Control Algorithm.....	52
4. Result and Discussion.....	55
4.1 Simulation Results	55
4.1.1 FEA Outcomes	55
4.1.2 CFD Outcomes	58
4.2 Prototype Testing	61
4.3 Integration to ROV Framework	65
5. Conclusion	66
6. Recommendation	67
References	68
Appendices	73

List of Figures

Figure 1: ROV inspecting underwater (Maritim Karriere, n.d.).....	1
Figure 2: Gantt Chart.....	5
Figure 3: ROV components (Christ & Wernli, 2007).....	7
Figure 4: Exploded view of magnetic thruster (Gucer et al., 2020).....	8
Figure 5: Hubless rim-driven thruster (Hsieh et al., 2007).....	9
Figure 6: Hybrid propulsion assembly (Scaradozzi et al., 2017)	9
Figure 7: Implementation of Thursters (Binugroho et al., 2018)	10
Figure 8: Circular ROV with thrusters (Salem et al., 2023).....	10
Figure 9: Particle robot walking and rolling (Mateos. 2020).....	13
Figure 10: Fin beat-cycle (Costa et al., 2022)	14
Figure 11: Assembled propeller with main body (Zhang et al., 2018)	15
Figure 12: Flow chart – Methodology	16
Figure 13: Flow chart – Mechanism	17
Figure 14: Lateral fin design.....	18
Figure 15: Superimposition curve (Bianchi et al., 2021)	19
Figure 16: Dorsal fin design	19
Figure 17: Seahorse fin muscles (Liu & Li, 2024).....	20
Figure 18: Caudal fin design	20
Figure 19: Cam-like mechanism (Costa et al., 2017)	21
Figure 20: Model of undulating fin (Low, 2009)	23
Figure 21: 3D printing components with PLA filament.....	28
Figure 22: 2D view - Frame	31
Figure 23: 2D view – Electronic Enclosure.....	32
Figure 24: 2D view – Thruster-Fin Assembly.....	32
Figure 25: Exploded view and B.O.M – Frame.....	33
Figure 26: Exploded view and B.O.M – Electronic enclosure.....	34
Figure 27: Exploded view and B.O.M – Thruster.....	35
Figure 28: Full CAD Assembly	36
Figure 29: FAST chart	37
Figure 30: Thruster system sub-assembly	38
Figure 31: Meshed body with boundary conditions	43
Figure 32: FEA pre-processing conditions.....	44
Figure 33: Meshed model inside water domain.....	45
Figure 34: Side view, front view and isometric view of prototype	51
Figure 35: Arduino code for motion	53
Figure 36: Von Mises stress	55
Figure 37: Resultant Displacement	56
Figure 38: Equivalent strain.....	57
Figure 39: Pressure plot	58
Figure 40: Velocity plot.....	58
Figure 41: Vorticity plot.....	59

Figure 42: Flowline plot with shear stress	59
Figure 43: Goals iteration graph.....	60

List of Tables

Table 1: ROV categories (Azis et al., 2012).....	7
Table 2: Comparison of total forward thrusts (Zhou & Zhao, 2020)	11
Table 3: Fault codes (Akmal et al., 2012)	11
Table 4: Constraint table.....	22
Table 5: Criteria Table.....	22
Table 6: Material Selection Table.....	30
Table 7: MCI Calculation	39
Table 8: Design for assembly	40
Table 9: FMEA Table	41
Table 10: Solution Table	42
Table 11: FEA pre-processing values	44
Table 12: CFD pre-processing parameters.....	45
Table 13: Fabrication Steps	46
Table 14: General Setup.....	61
Table 15: Waterproofing Test.....	62
Table 16: Buoyancy Test	62
Table 17: Maneuverability Test	63
Table 18: Thruster Performance Test	63
Table 19: Power Consumption Test.....	64

1. Introduction

This chapter introduces the context of the project by outlining the research motivation, defining objectives, and explaining scopes and limitations of the study. The structure of the report is also provided for guidelines.

1.1 Background

Remotely Operated Vehicles (ROVs) are indispensable tools in modern underwater exploration and operations. They are tethered and unmanned systems, widely used in offshore oil and gas industries. Historically, the dangerous tasks like underwater inspections and repairs were done by the well-trained divers. With the development of ROVs, the underwater applications became more convenient with little to no risks. Fields, such as marine engineering, naval defence and other scientific researches also utilize the ROVs for their subsea applications (Aguirre-Castro et al., 2019; Khojasteh & Kamali, 2017). However, conventional thrusters have limitations in directional control and energy consumption. These challenges necessitate innovation in propulsion mechanism of ROVs.

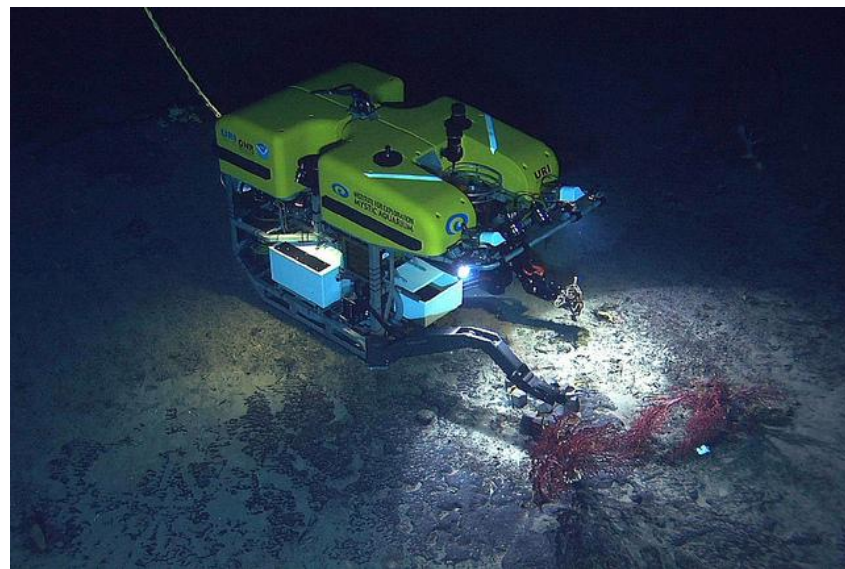


Figure 1: ROV inspecting underwater (Maritim Karriere, n.d.)

Inspired by nature's movements and navigations, biomimicry technology has emerged as an alternative to conventional propulsion systems. Designs imitating fish fins, whale tails and other aquatic locomotion patterns have become promising adaptations to ROV frames. This project investigates the integration of bio-inspired propulsion mechanisms into ROV thrusters by leveraging bio-principles. The study is expected to contribute to the developments of innovative underwater thruster designs that outperform conventional systems.

1.2 Problem Statement and Research Questions

The motivation of this research stems from the need to overcome the limitations of current designs. One of the main challenges faced by traditional thrusters is the manoeuvrability issues. They are difficult to maintain stability and take significant time to reach to the destination in turbulent currents. For instance, during deep-sea pipeline inspections, the inability to manoeuvre efficiently can lead to delay of the operation. This could further increase energy consumption overtime. Moreover, these designs generate noise pollution which disturbs marine ecosystems.

By contrast, marine animals such as fishes and squids have better agility and stability in similar conditions. Their flexible fins allow them to swim effectively. Adopting a bio-inspired thruster would enable ROVs to glide smoothly in harsh environments. Two key research questions that are intended to be solved are –

- (i) How can bio-inspired thrusters improve the manoeuvrability of ROVs, compared to conventional designs?
- (ii) Which integration features could address the problems while maintaining cost-efficiency and sustainability?

1.3 Aim and Objectives

Aim

The aim of the project is to design and optimize a bio-inspired thruster for ROVs to enhance efficiency, manoeuvrability and sustainability of ROV system.

Objectives

Three primary objectives to reach the aim of the projects are as follows.

- (i) To develop a thruster design based on the propulsion mechanisms of marine animals
- (ii) To test and validate the performance of prototype; in terms of energy efficiency and manoeuvrability under simulated underwater conditions
- (iii) To evaluate the design compatibility to existing ROV frameworks

1.4 Scope and Limitations

This study focuses on designing and testing a bio-inspired thruster for observation-class ROVs. The thruster design with oscillating fin mechanisms is fabricated for standard ROV frame. 3D CAD model of final selected design is assembled and simulated through Computational Fluid Dynamics (CFD). Along with a physical prototype, the experimental results are compared and validated. Additionally, design for manufacture and assembly, cost analysis, failure mode and effect analysis, and prototype data collection are performed to support the overall scope.

However, the study is limited to small-scale observation-class. This project mainly focuses on the thruster mechanisms and does not include the complete ROV system. Material selection for prototype is also constrained by budget and availability. Thus, the long-term durability testing may be impacted. Moreover, it should be noted that the performance testing in controlled water tank may not fully replicate the real-world subsea conditions.

1.5 Report Outline

This report is organized into six chapters, each of which details specific aspect of the project.

1. Introduction: This provides the introductory outline and structure of the report. The problems are identified and research motivation is revealed. The project timeline is identified with Gantt chart.
2. Literature Review: This chapter evaluates existing literature on ROV systems, thruster evolution, and bio-inspired technologies to justify the study.
3. Methodology: In this chapter, step by step approach for research and prototype fabrication are developed in details.
4. Result and Discussion: This chapter presents the findings from simulations and experimental tests. These are further analysed and compared with conventional values.
5. Conclusion: The project is summarized with key outcomes of the research data.
6. Recommendation: This is the suggestions towards potential improvements and implications for future ROV designs.

1.6 Gantt Chart

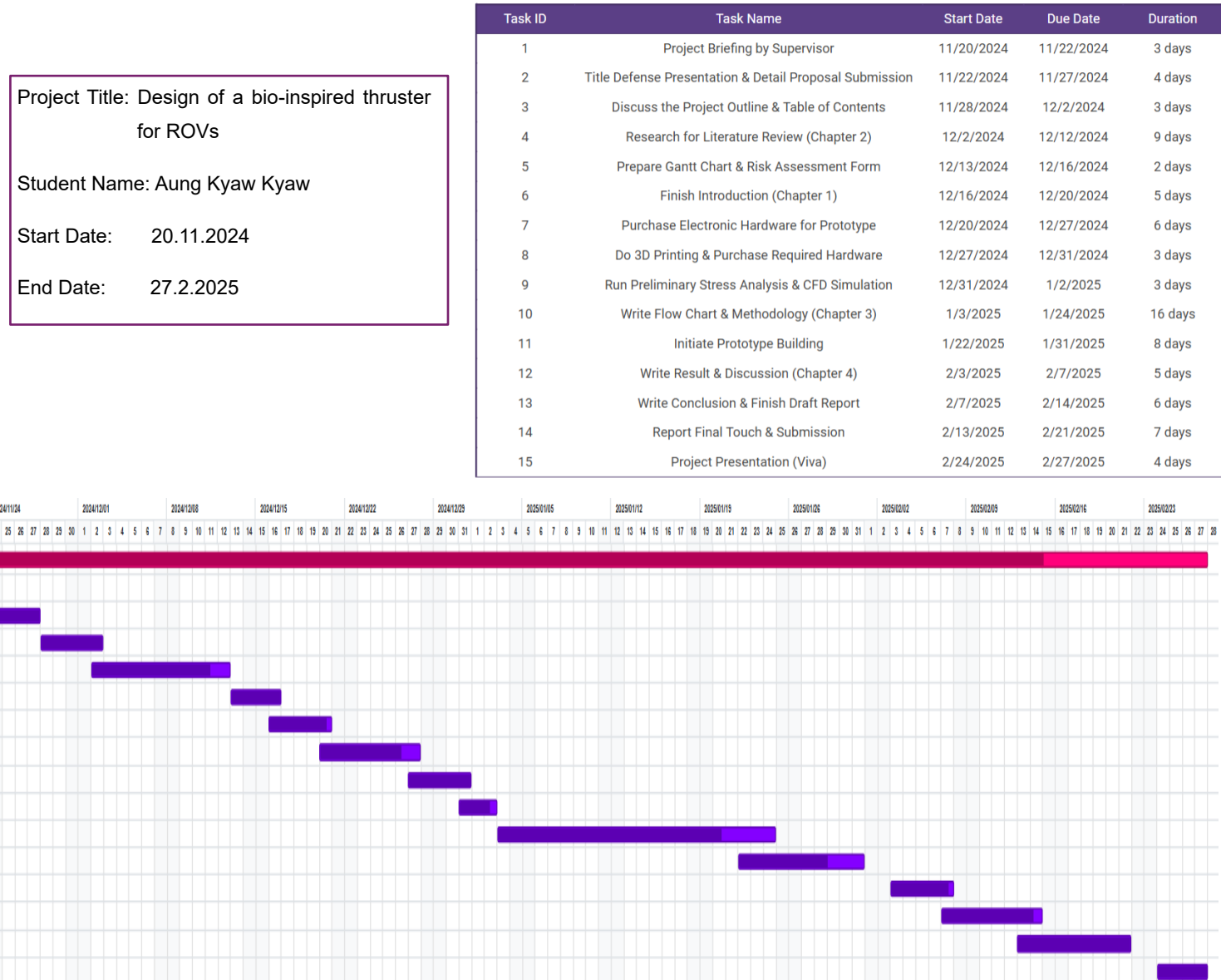


Figure 2: Gantt Chart

2. Literature Review

This chapter reviews and explores the advancements and challenges of ROV thrusters through time. It also highlights the evolution of bio-inspired robot designs, with their advantages and disadvantages.

2.1 Overview of ROVs

Remotely operated vehicles known as ROVs are underwater robots, connected to a control centre above water by a tether. This tether transmits commands and power to the ROV. It in turn resends sensor data and video imagery to the operator. ROVs carry out complex and dangerous subsea tasks that are risky for men. These tasks may include inspection, maintenance, repair, and construction in the offshore oil and gas sector; scientific research and data collection in marine biology and oceanography; exploration and recovery in underwater archaeology; and search, rescue, and surveillance operations in defense and security applications (Christ & Wernli, 2007). ROVs may not fully replace human divers but their capabilities to operate at greater depths and longer duration make them still better and safer choice. They are equipped with range of sensors, cameras, and manipulators for interaction, and are typically controlled by ROV pilots. As technology continues to advance, the role of ROVs is likely to expand further.

Basically, ROV system consists of following components:

- Frame: According to ROV manual, size range from 6 in × 6 in to 20 ft × 20 ft. Foam for buoyancy and ballast for gravity are attached above and below frame.
- Thrusters: Propellers, together with their relevant electrical counterparts are involved.
- Umbilical Cable: A tether that supplies power and communicates the vehicle with operator.
- Control Platform: Locates on a surface vessel for monitoring and control.
- Subsystems: Depending on specific mission, mechanical arms, cameras, sensors, lightings, and manipulators are included.

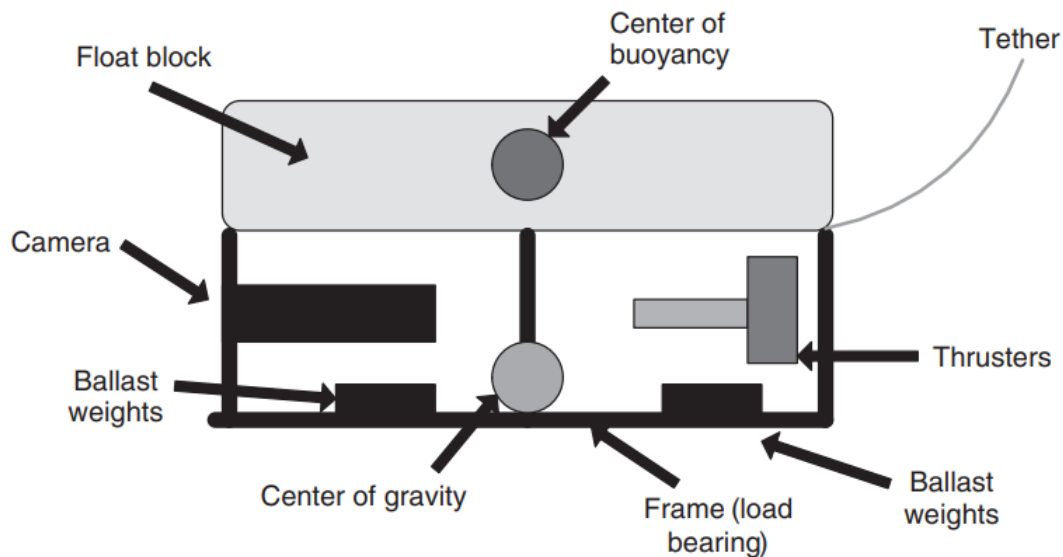


Figure 3: ROV components (Christ & Wernli, 2007)

ROVs are classified based on size, power system, and operational depth. Table 1 summarizes the capabilities of various ROV classes:

Table 1: ROV categories (Azis et al., 2012)

Class	Capability	Power (hp)
Low cost small ROV/ mini or micro ROV	Observation(<100 meters)	<5
Small ROV (Electric)	Observation (<300 meters)	<10
Medium (Electro/ Hydraulic)	Light/ Medium Heavy Work (<2,000 meters)	<100
High Capacity Electric	Observation/Light Work (<3,000 meters)	<20
High Capacity (Electro/ Hydraulic)	Heavy work/Large Payload (<3,000 meters)	<300
Ultra-Deep (Electric)	Observation/Data Collection (>3,000 meters)	<25
Ultra-Deep (Electro/Hydraulic)	Heavy Work/Large Payload (>3,000 meters)	<120

Frame used in this project falls under mini ROV category.

2.2 Review of Thrusters

ROV propulsion thrusters play critical roles in determining the vehicle's manoeuvrability, energy efficiency and operational effectiveness. Generally, traditional thrusters are classified into two main types, based on their power source; electric and hydraulic systems. Whether the system, thrusters should be able to move the vehicle in at least two directions; forward/backward horizontally and upward/downward vertically.

Propellers in Wageningen B-screw series have skew, rake and rounded blade tips (Fotland, 2018, p. 33). They emphasized the efficiency in open-water performance through different propeller geometries. Thus, the designs inspired by this series may not translate well to the underwater robots.

In the study of thrusters for mini class ROVs by Gucer et al. (2020), brushless DC motor with magnetic coupling transmission element were used (Figure 4). The results showed that design can be operated up to 100 meters depth. A smaller thruster may reduce drag but it is difficult to provide adequate thrust. Rosid et al., 2018 disassembled the thruster and employed the reverse engineering approach. This helps in identifying the area for performance improvement. The optimized design illustrated a 2% increase in static thrust and 7% decrease in input power compared to original design.

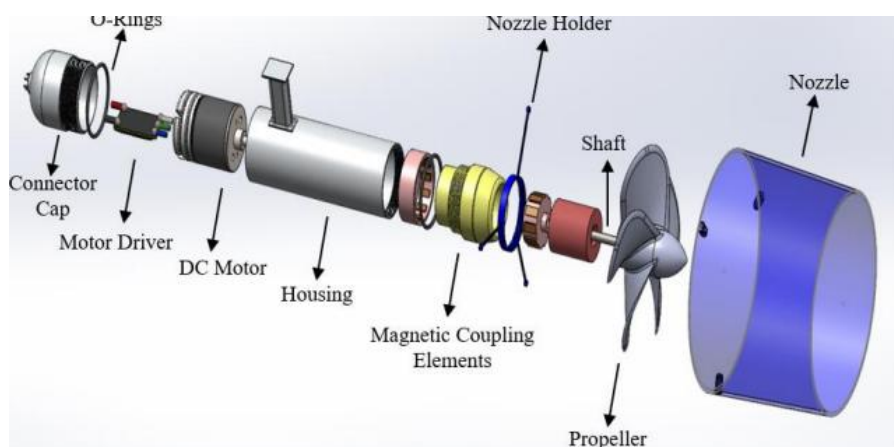


Figure 4: Exploded view of magnetic thruster (Gucer et al, 2020)



Figure 5: Hubless rim-driven thruster (Hsieh et al., 2007)

In order to avoid the entanglement of foreign matters, “hubless” thrusters were introduced (Hsieh et al., 2007). As shown in Figure 5, their motors are constructed as rim and embedded into the duct. Friction on bearings and insufficient current were encountered but the simulation performance was acceptable.

Advancements have introduced counter-rotating dual-propeller system. They eliminate gyroscopic moments and hence, provide vibration-free operation. Together with the hydraulic system, dynamic positioning is easily capable and are ideal for military applications (DeWijs, 2000). Ducted thrusters, currently most used ones can increase thrust at low speeds. They reduce the risk of propeller damage in cluttered underwater environments.

Hybrid propulsion systems were tested later. In BRAVe vehicle, caudal fin thruster is used for energy efficiency while typical horizontal and vertical thrusters are combined for directional control (Scaradozzi et al., 2017).

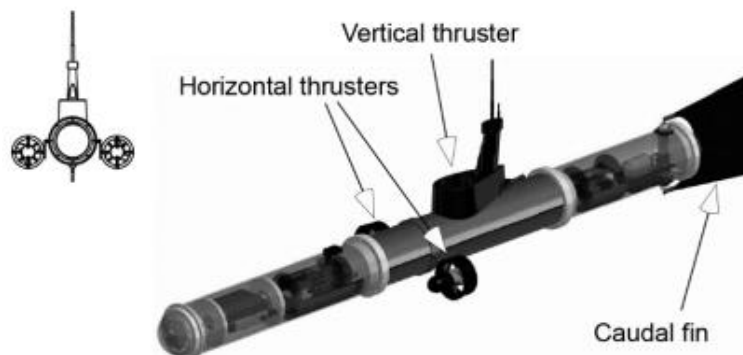


Figure 6: Hybrid propulsion assembly (Scaradozzi et al., 2017)

2.2.1 Thruster Configuration

At present, ArduSub controller can handle the configuration from 3 up to 8 thrusters (Binugroho et al., 2018). As Figure 7, thrusters are located based on ROV designs and purpose. Leading ROV producers like BlueRobotics and TT Robotix both use these configurations in their vehicles. Unique frame design with circular shape also positions the propellers in similar as shown in Figure 8. This allows easy rotation and turbulent flow reduction (Salem et al., 2023).

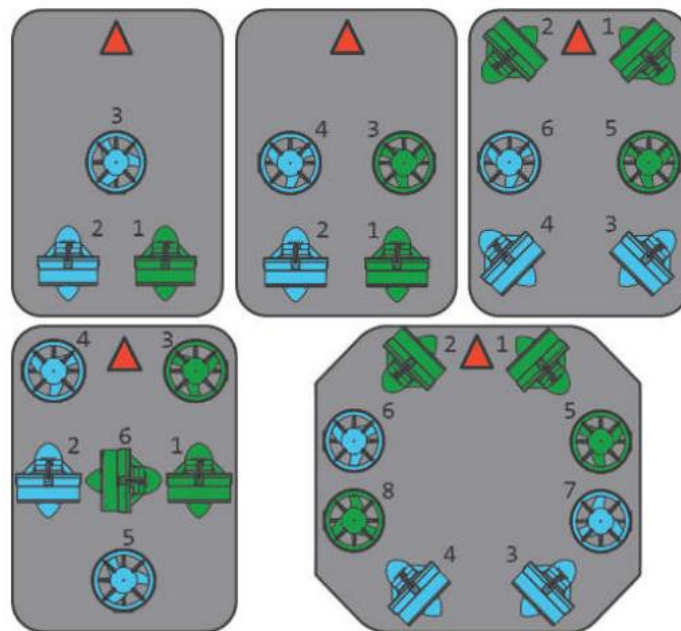


Figure 7: *Implementation of Thrusters (Binugroho et al., 2018)*

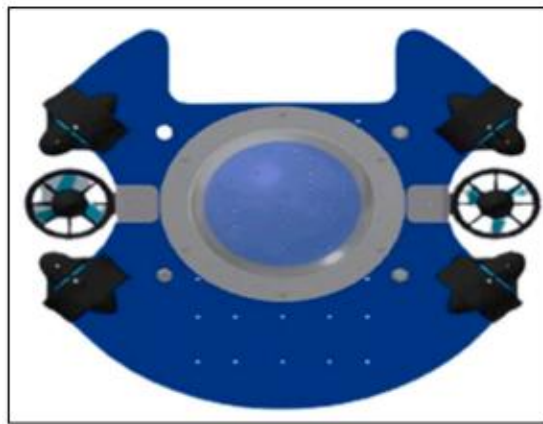


Figure 8: *Circular ROV with thrusters (Salem et al., 2023)*

2.2.2 Manoeuvrability Challenges

The thruster configurations have the great influence on the vehicle's manoeuvrability. The number and strategic placement of thrusters determine the overall performance for reaching the destination. Improper positioning may lead to insufficient thrust vectors. Moreover, thruster-thruster interaction is also significant and complex for propulsion system. Due to the interaction, certain deflection angles are forbidden and deviations need to be considered (Zhou & Zhao, 2020). This further limits the precise movement underwater. The interaction and thrust force are calculated for four thruster arrangements in Table 2.

Table 2: Comparison of total forward thrusts (Zhou & Zhao, 2020)

	820 rpm	1200 rpm
Forward thrust of one side (N)	2194.23	4678.07
Forward thrust of one side (N) $\times 2$	4388.46	9356.14
Total forward thrust of four-thruster arrangement (N)	4374.02	9243.81
Δl (N)	14.44	112.33
Interaction (Δl /Total forward thrust of four-thruster arrangement)	0.33%	1.22%

Under design constraints, typical ROVs also face challenges in determining the optimal configuration for damping matrix, restoring forces and moments, and body force from actuators (Gomes et al., 2005). These parameters are all responsible for the motion of underwater vehicle. Additionally, hydrodynamic forces, including drag, lift, and buoyancy are all influential factors for ROV speed and directional control.

In the case of finding thrusters fault, it is quite challenging to determine the exact cause (Akmal et al., 2012). The common fault types that have impact on manoeuvrability are listed in Table 3.

Table 3: Fault codes (Akmal et al., 2012)

Thruster state	Class	Type	Constraint bound s_i
Normal (fault free)	-	-	1.0
Partially blocked ducting	External	Partial	0.8
Fully blocked ducting	External	Total	0
Voltage increase	Internal	Partial	0.7
Voltage drop	Internal	Partial	0.9
Voltage total loss	Internal	Total	0
Unknown	Internal	Total	0

2.3 Bio-inspired Technology

Bio-inspired technology has developed into innovative engineering systems by mimicking structures and principles observed in nature. In robotics, these designs compete the traditional mechanisms and expect to overcome the existing drawbacks.

2.3.1 Aboveground Bio-inspired Robots

Various aboveground robots have emulated the specific animal behaviours and morphologies. Some of the updated and notable projects are as follows.

(i) Giraffe Neck Robot

This robot draws inspiration from unique musculoskeletal structure of a giraffe's neck. It shows remarkable strength and flexibility. With the intention to reproduce its range of motion and robustness, it is useful in disaster sites or forest industries (Niikura et al., 2022).

Despite the advantages of high adaptability and structural efficiency, the design is complex and scaling for larger models have difficulties in time and cost.

(ii) Robotic Cat

Biologically inspired robotic cat was developed for research and educational purposes. This robot can run and avoid the obstacles autonomously, as well as be controlled by Bluetooth (Abrar & Islam, 2020).

The project offers a hand-on platform for learning biomechanics and robotics. The design also provides data for quadrupedal locomotion but it lacks the robustness for industrial applications.

(iii) Particle Robots

More interestingly, there are studies and development of robots inspired just by simple particle-like organisms. This bionic robot as shown in Figure 9, is designed to be adaptable for multiple environments, while mechanically modular and efficient (Mateos, 2020).

They are versatile as they can both walk and roll with spherical body. Control system is also accessible but operating dual locomotion can lead to high energy consumption.

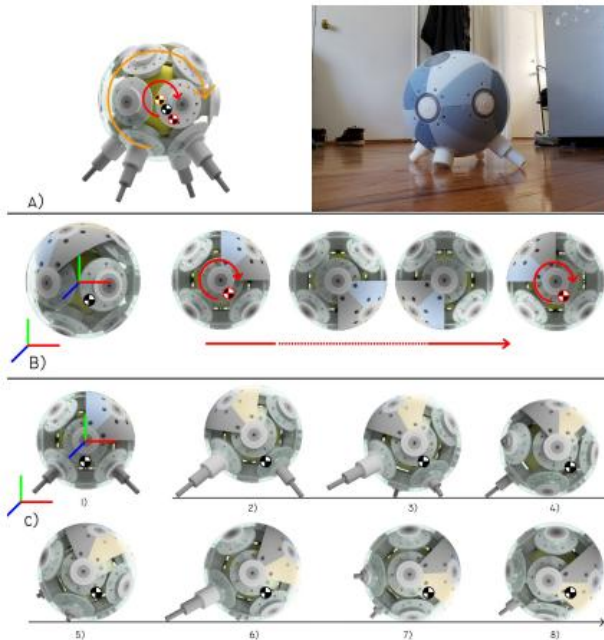


Figure 9: *Particle robot walking and rolling* (Mateos. 2020)

2.3.2 Underwater Bio-inspired Robots

Biomimicry is more approachable topic in underwater vehicles. Movements of marine animals such as whales, squids, and even octopus tentacles have been well adapted into certain mechanical products. In this section, bio-propulsion mechanisms are emphasized in order to compare as market research for the project's design.

(i) HERO-BLUE

This robot has a multimodal fin with numerous joints that can either swim, crawl, or even walk (Kim et al., 2024). It combines various movement strategies of aquatic animals including salamanders. This robot is constructed for hazardous environments.

Versatility and manoeuvrability are supreme for this design but switching between different movements may lead to high energy consumption and design complication.

(ii) Labriform-Steering Robot

This vehicle adopted blade element and drag-based labriform swimming, with the aim of improving manoeuvre-capability by novel transmission system (Costa et al., 2022). Cycles of power strokes and recovery strokes are achieved as in Figure 10.

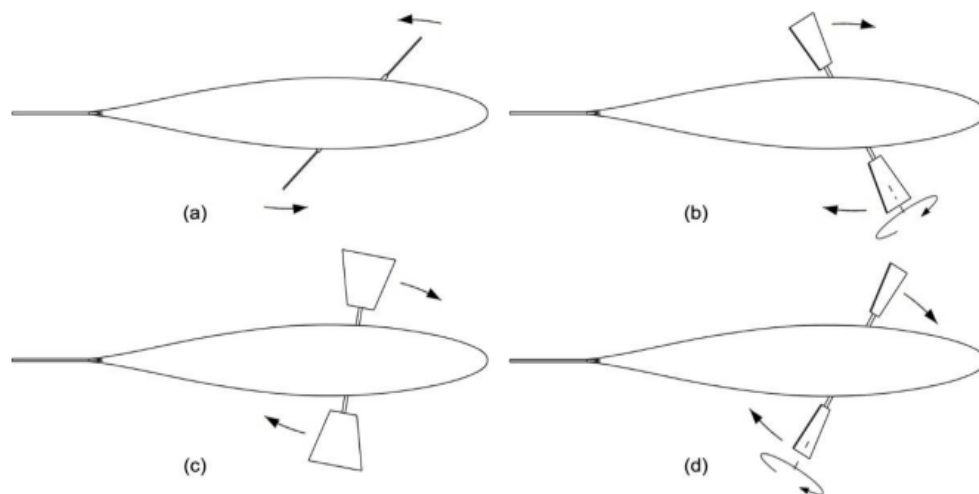


Figure 10: *Fin beat-cycle* (Costa et al., 2022)

The use of single motor or rotary flapping mechanism simplifies the concept and propulsion efficiency is improved. However, speed is limited and applications with rapid movement may debug the vehicle.

(iii) Mantra Ray Propellers

The movement of pectoral fins based on rigid mechanism and flexible bladder, is similar to bird flapping mechanism but more authentic (Zhang et al., 2018). Based on the experiments on this, the authors concluded the validity of their design and smooth transition modes between each stroke. The mechanical structure of the propeller is shown in Figure 11.

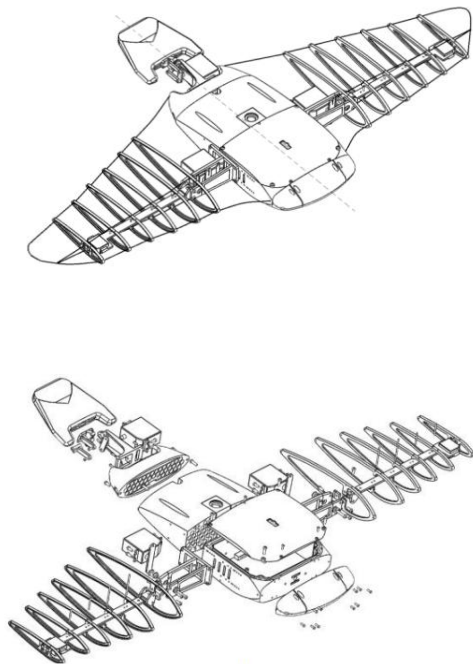


Figure 11: Assembled propeller with main body (Zhang et al., 2018)

Other similar concepts were also introduced in recent years, proving that the traditional mechanisms are not only solution to obtain the device's full potential. With these underlying improvements, the proposed design will be constructed and simulated in next chapter.

3. Methodology

3.1 Flow Chart

Firstly, a flow chart for the methodology is established from design thinking to data collection before discussion chapter. The working principle and experimentation of prototype is also analysed in a separate flow chart (Figure 13).

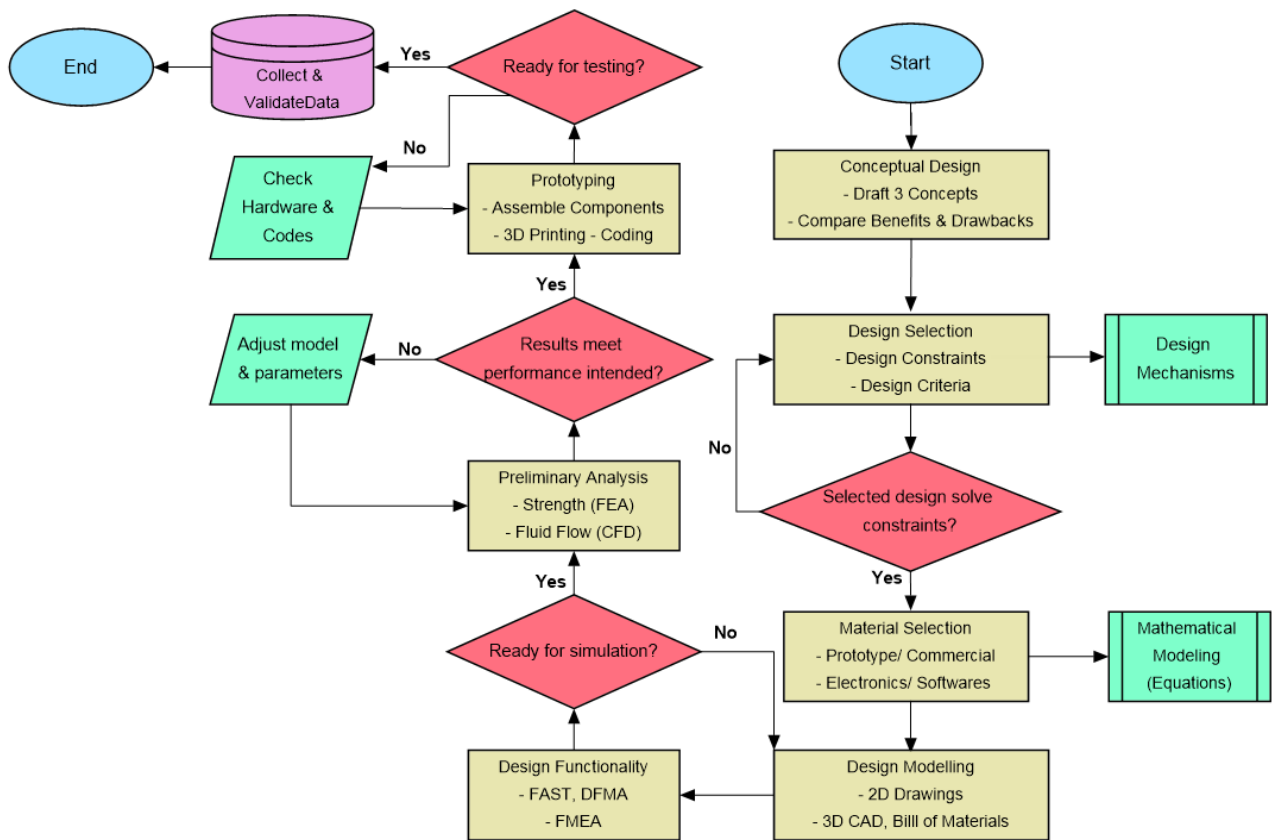


Figure 12: Flow chart – Methodology

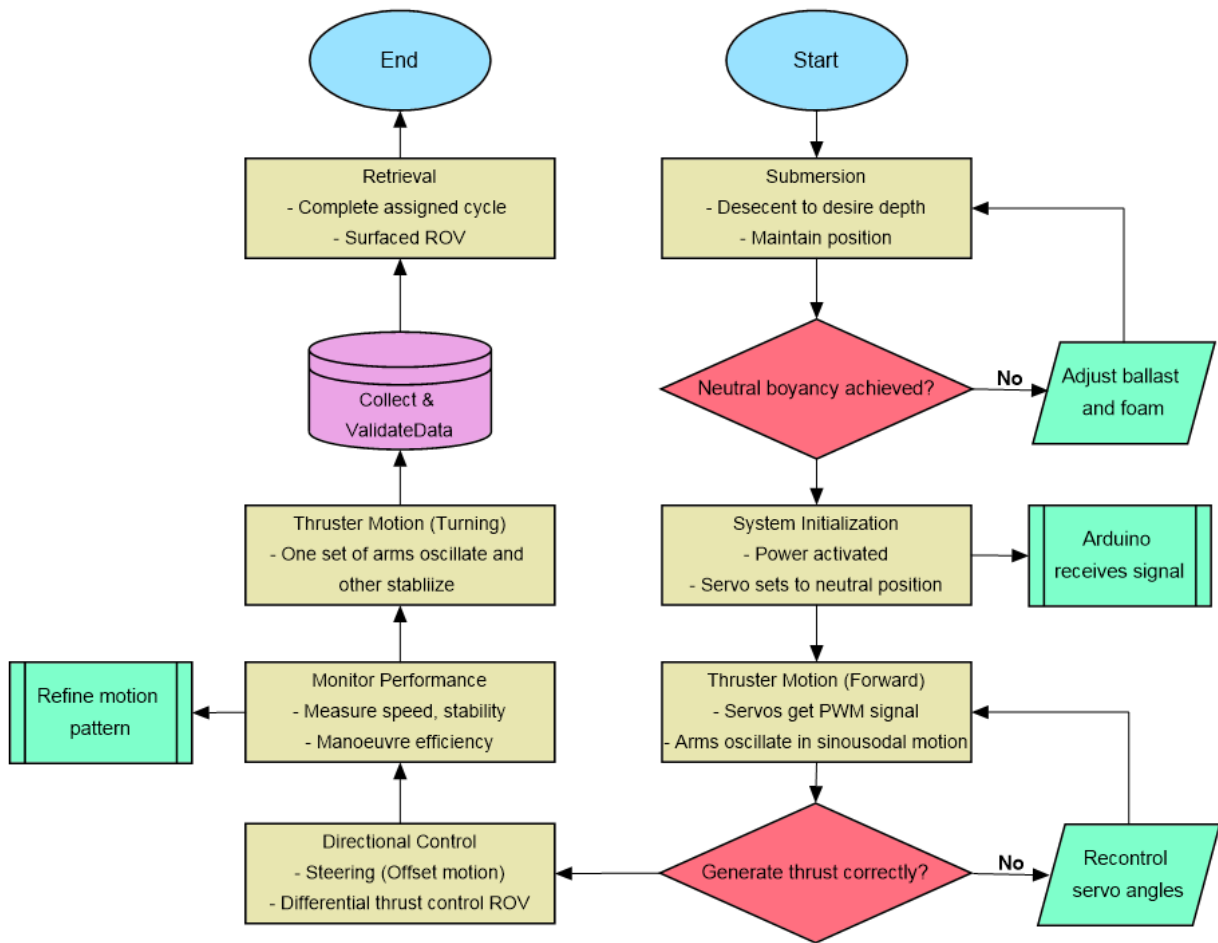


Figure 13: Flow chart – Mechanism

3.2 Conceptual Designs

This section analyses the designs that focus on translating unique movement patterns of aquatic animals into mechanical systems. Three proposed concepts with the draft CAD models are presented; they are then undergone design constraints and criteria selection. The final design is selected in the end before moving forward to simulation and prototyping.

3.2.1 Concept 1 – Cownose Ray-Inspired Linkage Mechanism

This concept is inspired from motion of cownose rays. Their fins move in smooth oscillatory pattern to achieve propulsion. The external surface is shown in Figure 14, where the internal system includes four-bar linkage mechanism. At the core, a motor drives the input link. This initiates a continuous rotary motion, which alternately moves the series of linkages via sliders and hinges. Then, final movement is given to the output link connected to the center of the fin. As a result, the fins oscillate in controlled manner as observed in cownose rays.

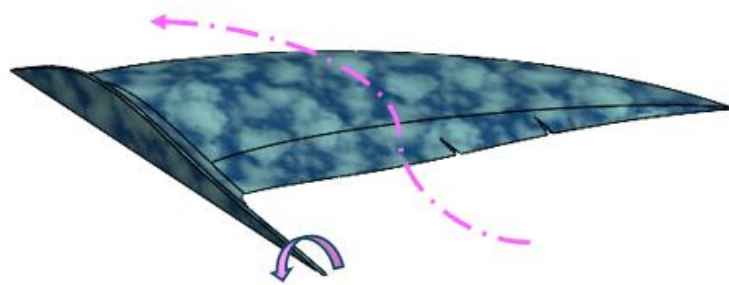


Figure 14: *Lateral fin design*

The linkage connections and central cross-section of cownose ray are superimposed in the fin span curve made by Bianchi et al., 2021. This can be seen in Figure 15.

For benefits, the design aims to maximize mechanical precision and durability. However, components are intricate and careful maintenance is required. Moreover, due to friction, there is a potential for energy losses.

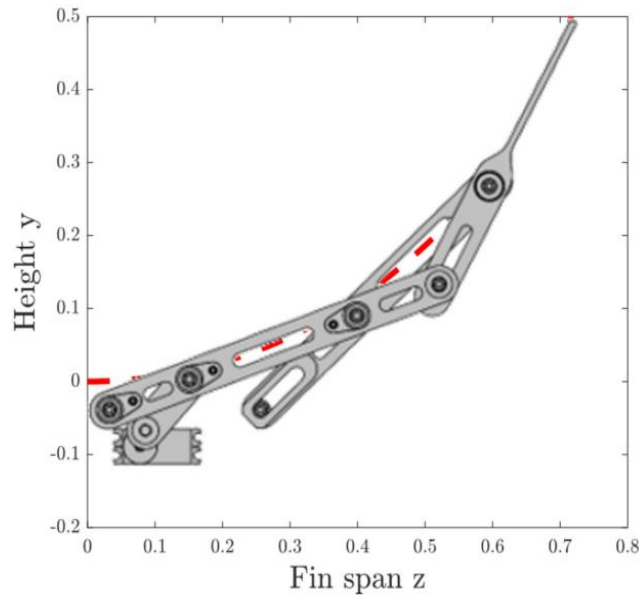


Figure 15: *Superimposition curve (Bianchi et al., 2021)*

3.2.2 Concept 2 – Seahorse-Inspired Oscillating Fin Mechanism

This concept takes inspiration from finely coordinated movements of seahorses. The tilt link control with servo driver design is shown in Figure 16.

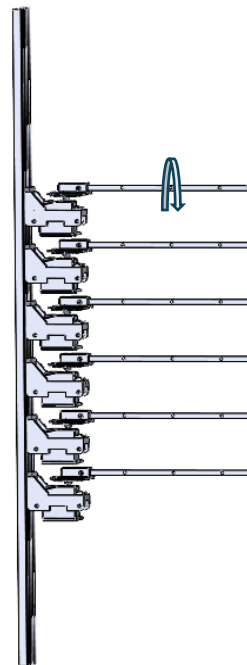


Figure 16: *Dorsal fin design*

In operation, 180° servo motion is transmitted to connecting rod. Then, the attached fins produce back-and-forth movements individually. The synchronized tilting of all fin rays resulted in a smooth and wave-like motion. This is similar vertically to the dorsal fin inclination of seahorses. The fins connected to spine have two muscles groups: Muscle 1 controls the pitch and inclination, while Muscle 2 is responsible for oscillation and conventional movements (Liu & Li, 2024).

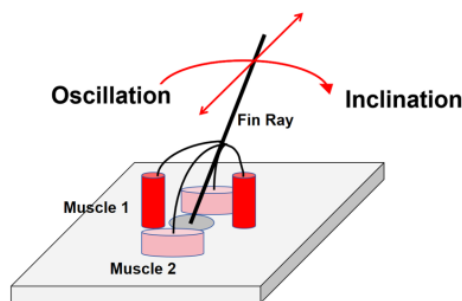


Figure 17: Seahorse fin muscles (Liu & Li, 2024)

The horizontal alignment of this structure can minimize drag, while maximizing thrust efficiency. The compact design with low drag characteristics makes this mechanism appealing for ROV applications. The efficient use of space also ensures minimal disruption to overall vehicle design. However, the system requires careful waterproofing and calibration to enhance reliability.

3.2.3 Concept 3 – Fish Tail-Inspired Cam-Like Mechanism

Unlike other designs, this mechanism relies on constant velocity input. The tail flapping is mimicked from fish caudal fin. As seen in Figure 18, the design features driving disk, rotational sphere, hinge and tailboard. The rotation is along the hinge axis.

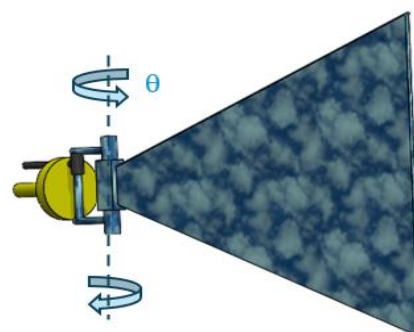


Figure 18: Caudal fin design

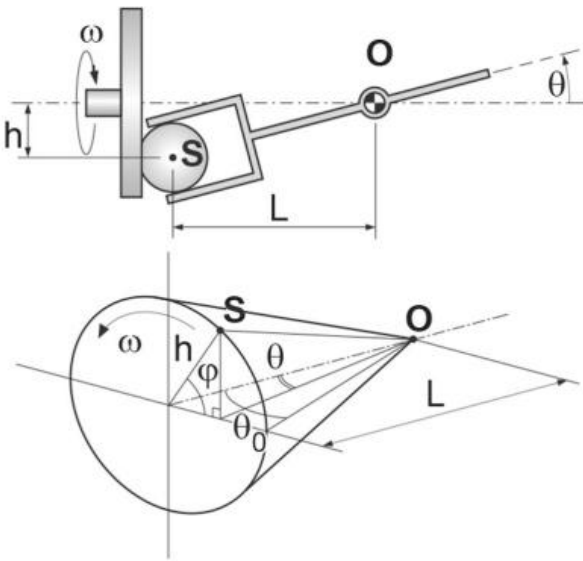


Figure 19: *Cam-like mechanism (Costa et al., 2017)*

The cam-like mechanism simplifies the control requirements. This eliminates the need for complex position adjustments. According to Figure 19, the output shaft is connected to the driven member and able to pivot freely (Costa et al., 2017). The authors stated that mechanical efficiency of the cam-like mechanism is 79.2%.

Advantages include simplicity, frictionless efficiency and ideal for steady navigation. On the other hand, rapid directional switch is limited and flexibility is lack in confined or tight environments. The design also needs additional side propellers for precise manoeuvring.

3.2.4 Design Constraints

After sketching three potential conceptual designs, the most suitable design for further development is determined. The first approach is a constraint filter. The only concept that meets all the critical constraints proceed to next stage.

Table 4: *Constraint table*

Concept	Constraints					Judgement
	Arduino Compatibility	Sufficient Thrust	Less Space Requirement	Ease of Manufacturing (Fins)	Integration to ROV Frame	
1	NO	YES	NO	YES	YES	✗
2	YES	YES	YES	YES	YES	✓
3	YES	NO	YES	YES	NO	✗

Outcome: Concept 2 satisfies all constraints and progress to next phase.

3.2.5 Design Criteria

The criteria table is a weighted evaluation against each concept. By assigning weightage values (1-10), overall grade score for each concept is rated. It is calculated by multiplying the weightage and rating. The total score for all criteria is summed up.

Table 5: *Criteria Table*

Criteria	Weightage (1-10)	Concept 1		Concept 2		Concept 3	
		Rating (1-10)	Grade	Rating (1-10)	Grade	Rating (1-10)	Grade
Manoeuvrability	9	7	63	7	63	5	45
Thrust Efficiency	8	7	56	7	56	6	48
Ease of Assembly & Integration	7	5	35	6	42	6	42
Control Simplicity	6	5	30	7	42	6	36
Cost-effectiveness	5	5	25	5	25	6	30
Total		209		228		201	

Outcome: Concept 2 achieves the highest total score. It is therefore considered as the final design.

3.2.6 Final Design Selection

According to the constraint and criteria tables, concept 2 outperformed the other two. While assembly may require precision, it is still flexible and controllable by Arduino. Thus, it is optimal choice for both simulation and prototyping.

Underwater vehicles should mount at least two fins in order to enhance manoeuvrability (Shang et al., 2012). In their AUV design, the authors tested with 10 fin rays on both sides. In the study with fishlike side-fins by Toda et al. (2004), 15 fin bones were used to emulate the undulating motion.

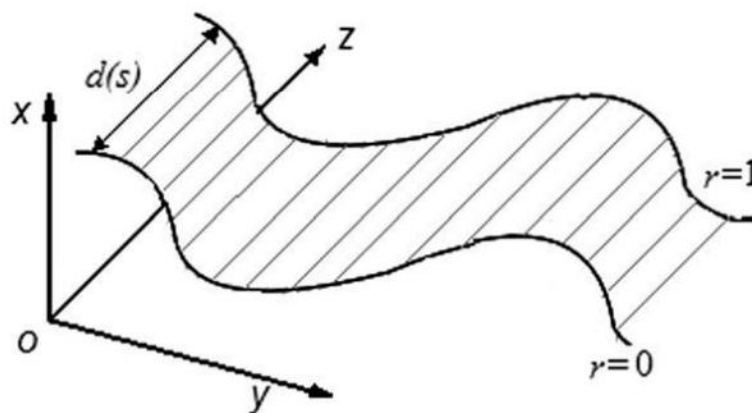


Figure 20: Model of undulating fin (Low, 2009)

The final design for this project includes only two fin rays on each side. This reduction simplifies the mechanical structure and control system. It can still maintain the balance between thrust generation and structural manageability. With the use of only four servo motors, the attached two fin rays on each side are to move in a sinusoidal pattern. The fins are connected by the flexible sheet in between. The wave-line motion is expected to translate along the sheet. When the first fin leads and the second fin lags, the sheet flexes into an arc. As the fins oscillate, this arc alternates direction. This creates thrust-generating flapping motion.

The design has to fulfil the functionality, where simplicity and practicality are also important factors. Detailed connections, specifications, and kinematic equations will be discussed in upcoming sections.

3.3 Kinematic and Dynamic Modelling

The mathematical equations regarding the selected design and its mechanisms are stated in this section.

3.3.1 Fin Shape and Motion

The fin's displacement at any point along its length can be modelled as:

$$z(x, t) = \begin{cases} A_0(x) \sin(2\pi NT - 2\pi x/L) & \text{if } \sin(2\pi NT - 2\pi x/L) \geq 0 \\ 0 & \text{if } \sin(2\pi NT - 2\pi x/L) < 0 \end{cases}$$

Where:

- $A_0(x)$: Amplitude distribution along the fin, varies based on the relative position.
- N: Oscillation frequency
- T: Time
- L: Length of the fin
- x: Position along the length of the fin

For parabolic amplitude distribution:

$$A_0(x) = -0.024 \left(\frac{x}{L} - 0.5 \right)^2 + 0.0275$$

3.3.2 Servo Motion

The vertical oscillation of each fin's servo is:

$$\theta(t) = \arcsin \left(\frac{z(x, t)}{L_s} \right)$$

Where:

- $z(x, t)$: Fin displacement
- L_s : Distance from servo to fin's attachment point

Angular velocity of the servo controlling the fin is:

$$\dot{\theta}(t) = \frac{\partial}{\partial t} \arcsin \left(\frac{z(x, t)}{L_s} \right)$$

For $z(x, t) = A_0(x) \sin(2\pi NT - 2\pi x/L)$:

$$\dot{\theta}(t) = \frac{\cos(2\pi NT - 2\pi x/L)}{\sqrt{1 - \left(\frac{A_0(x)}{L_s} \sin(2\pi NT - 2\pi x/L) \right)^2}} \cdot \frac{\partial z(x, t)}{\partial t}$$

3.3.3 Fin Thrust Force

Thrust generated by fins can be estimated as:

$$F = C_T \rho A_{\text{fin}} v^2$$

Where:

- C_T : Thrust coefficient
- ρ : Density of water
- A_{fin} : Effective area of the fin
- v : Water velocity induced by fin oscillation

3.3.4 Fin Drag Force and Lift Force

The hydrodynamic drag force acting on the fins can be expressed as:

$$F_D = \frac{1}{2} C_D \rho A v^2$$

Where C_D is drag coefficient.

The force generated by fin's oscillatory lift is:

$$F_L = \frac{1}{2} C_L \rho A v^2$$

Where C_L is lift coefficient.

3.3.5 Servo Energy Consumption

Power consumption by each servo is:

$$P = \tau \cdot \omega$$

Where:

- τ : Torque required to move the fin
- ω : Angular velocity of the servo motor

3.3.6 Degrees of Freedom

Degrees of freedom (DOF) of the final design include the motions of each fin in response to hydrodynamic forces and servo actuation. Six potential movements can be represented as follows.

- Translational DOF: Surge (x), Sway (y), Heave (z)
- Rotational DOF: Roll (ϕ), Pitch (θ), Yaw (ψ)

DOF state vector 'q' is then,

$$\mathbf{q} = \begin{bmatrix} x \\ y \\ z \\ \phi \\ \theta \\ \psi \end{bmatrix}$$

In a case with pitch-dominated motion, the dynamic equation can be generated in matrix form.

$$\begin{bmatrix} m & 0 & 0 & 0 & 0 & 0 \\ 0 & m & 0 & 0 & 0 & 0 \\ 0 & 0 & m & 0 & 0 & 0 \\ 0 & 0 & 0 & I_{xx} & 0 & 0 \\ 0 & 0 & 0 & 0 & I_{yy} & 0 \\ 0 & 0 & 0 & 0 & 0 & I_{zz} \end{bmatrix} \begin{bmatrix} \ddot{x} \\ \ddot{y} \\ \ddot{z} \\ \ddot{\phi} \\ \ddot{\theta} \\ \ddot{\psi} \end{bmatrix} + \begin{bmatrix} d_x & 0 & 0 & 0 & 0 & 0 \\ 0 & d_y & 0 & 0 & 0 & 0 \\ 0 & 0 & d_z & 0 & 0 & 0 \\ 0 & 0 & 0 & d_\phi & 0 & 0 \\ 0 & 0 & 0 & 0 & d_\theta & 0 \\ 0 & 0 & 0 & 0 & 0 & d_\psi \end{bmatrix} \begin{bmatrix} \dot{x} \\ \dot{y} \\ \dot{z} \\ \dot{\phi} \\ \dot{\theta} \\ \dot{\psi} \end{bmatrix} = \begin{bmatrix} \tau_x \\ \tau_y \\ \tau_z \\ \tau_\phi \\ \tau_\theta \\ \tau_\psi \end{bmatrix}$$

Where:

- m : Mass of the ROV
- I_{xx}, I_{yy}, I_{zz} : Moments of inertia in roll, pitch, and yaw
- $d_x, d_y, d_z, d_\phi, d_\theta, d_\psi$: Damping coefficients in each DOF
- T_x, T_y, T_z : Forces acting on the ROV
- T_ϕ, T_θ, T_ψ : Moments generated by the fins

This matrix shows how forces and torques from thrusters influence the ROV's motion.

3.4 Material Selection

3.4.1 Frame Material

The selected material for the prototype frame design is PVC. PVC pipes are lightweight and resistant to water absorption (Kökçan & Tamer, 2020). They provide sufficient structural integrity and also flexibility for experimental adjustments. Due to their buoyant nature, the instant need for additional foams is also reduced. Modifications and adjustments during prototyping phase can also be done easily with PVC pipes and joints.

In real-life operations, marine grade composites are used for frame, depending on the operational depth and mechanical loads. However, PVC is still an ideal choice for current design.

3.4.2 Thruster Material

The components for thruster system are 3D printed with Polylactic Acid (PLA) filament. From motor brackets to fins and horns, PLA with at least 50% infill capacity is used. Ease of fabrication and customization during/after testing are important factors here. Thus, all the required parts are printed with care to maintain rigidity and flexibility. For the fin itself, the aluminium sheets are used and attached with PLA horn for better connection.

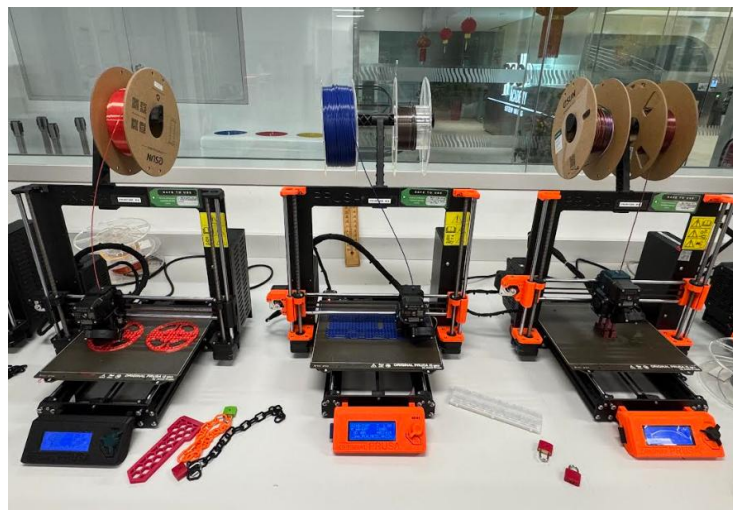


Figure 21: 3D printing components with PLA filament

Silicone rubber is used for the connection sheet between two fins. The sheets are expected to replicate biological fin movement in half arc-wave form.

For real applications, fins must be upgraded to carbon fibre rods, and rubber sheets to reinforced elastomers or composites. Materials are required to be stiff, fatigue and wear resistant, in order to work under continuous oscillations in harsh underwater environments.

3.4.3 Electronics Enclosure & Components

The waterproof enclosure for the prototype is a DIY PVC tube with end caps. They are chosen due to their affordability and ease of modification. Seals are created with silicone gaskets and cable glands. The electronics include:

- Arduino UNO (for motion control)
- Four DS15MG-180 IP67-rated waterproof servos (for thruster actuation)
- 6V 4000 MAh Sealed Lead Acid (SLA) battery (servos power source)
- 12V battery and voltage regulator (Arduino power source)
- Wire connectors and splitters (for power and signal transmission)
- Jumper wires and waterproof joints (for long-wired connections)

The 3D printed tray and clamps are inserted inside the tube for electronics stability and wiring flexibility.

For commercial model, IP68 waterproof enclosure with adjustable cable glands for wires and tether (that seen in BlueROV's enclosure module) should be installed. A custom housing with pressure-compensated enclosure is necessary. Brushless DC motors are also better replacements for servos in lifespan and efficiency.

3.4.4 Buoyant Foams, Ballasts & Miscellaneous Components

The prototype uses additional closed PVC pipes as required to act as foams. They are easy to shape and add or remove accordingly as required. Aluminium 6061 plate used for base of the ROV acts as both enclosure holder and ballast at the same time. Extra blocks are cut to serve as surplus weights. Foams and ballasts are adjusted to achieve neutral buoyancy. Centre of buoyancy is needed to maintain directly above centre of gravity (Christ & Wernli, 2007). In fully operational ROV, syntactic foams and floodable ballast chambers are replaced.

Other components such as zip ties, fasteners, screws and washers, bearings, silicone sealants, and rubber tubing are all standard materials available in market. The summarized table for material selection, comparing both operational versions is as below.

Table 6: *Material Selection Table*

Component	Prototype Material	Real-World Model Material
Frame	PVC pipes	Marine-grade aluminum / Carbon fiber composite
Thruster Housing	3D-printed PLA	Marine-grade ABS / Fiberglass
Flexible Sheet	Silicone rubber	Reinforced silicone composite / Polyurethane elastomer
Fin Supports	PLA rods	Carbon fiber rods
Electronics Enclosure	DIY PVC pipe	IP68-rated polycarbonate/aluminum housing
Actuation (Motors)	DS15MG-180 waterproof servos (IP67)	Brushless DC motors with sealed housings
Battery	Sealed Lead Acid (SLA)	Custom pressure-compensated battery pack
Buoyancy Material	PVC foam blocks	Syntactic foam
Ballast	Aluminum sheets	Variable ballast system / Floodable chambers
Miscellaneous	Market-available materials	Titanium fasteners, marine-grade conduits

3.5 Functional Assembly Model

The full model consists of three main sub-assemblies: ROV frame, electronics with the enclosure, and the thruster-fin assembly. Their 2D drawings, 3D models, and exploded view with bills of materials will be included in this section.

3.5.1 2D Drawings

Standard 2D views (top, front, & right-side) and their respective dimensions in MMGS system are illustrated for main sub-assemblies. The measurements of each separate part (pipes, joints, motor, etc.) are attached in Appendices.

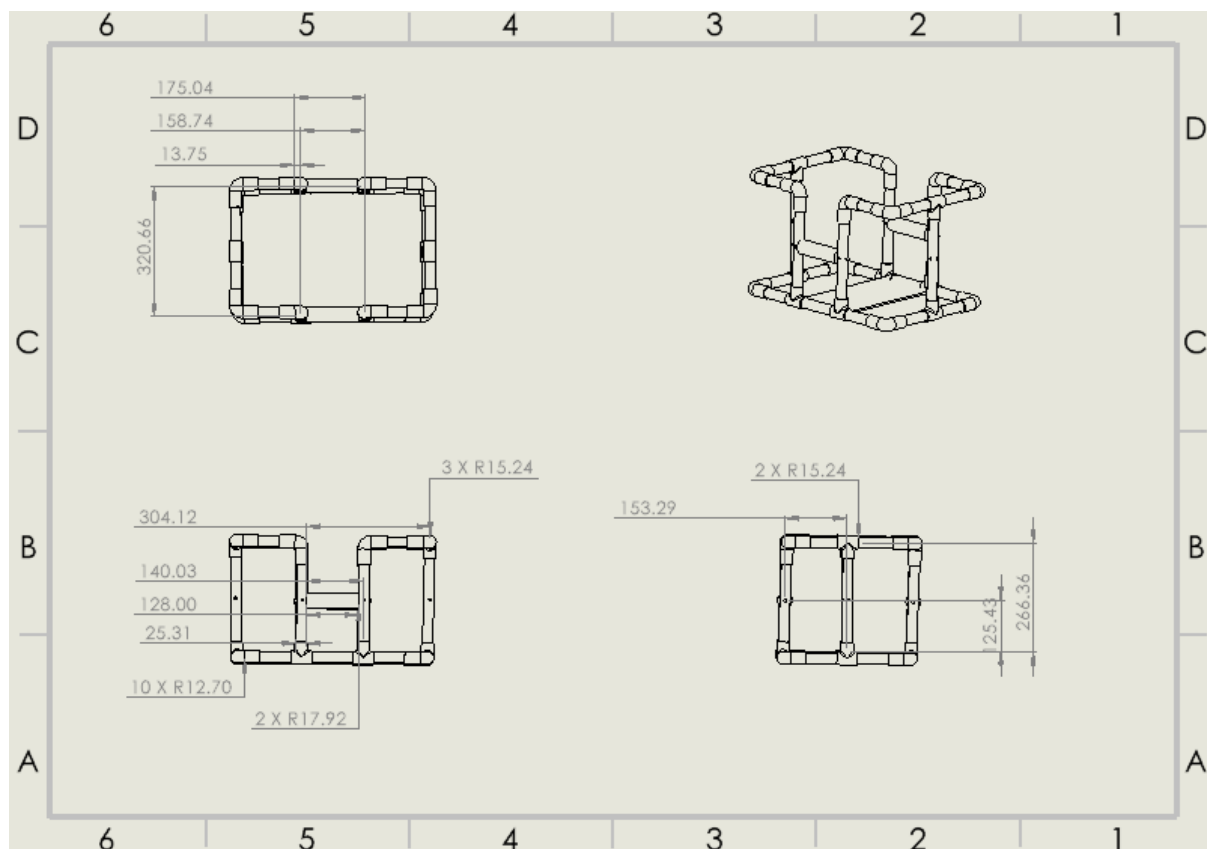
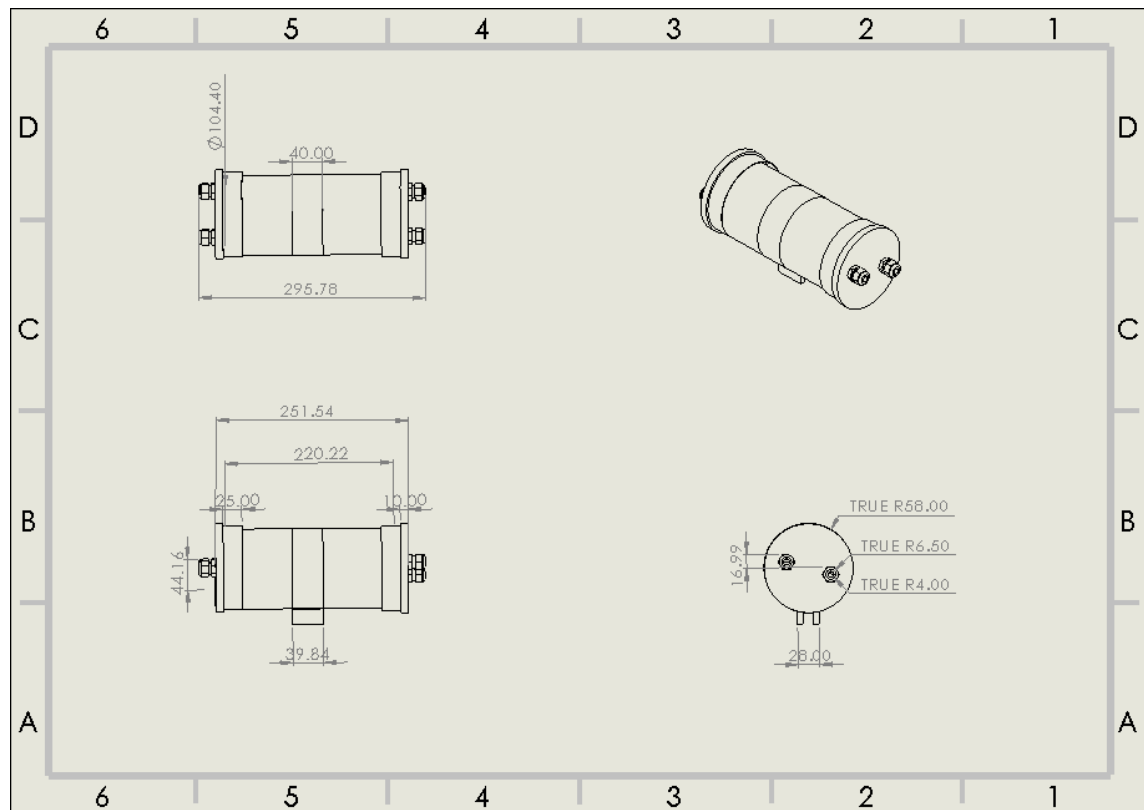
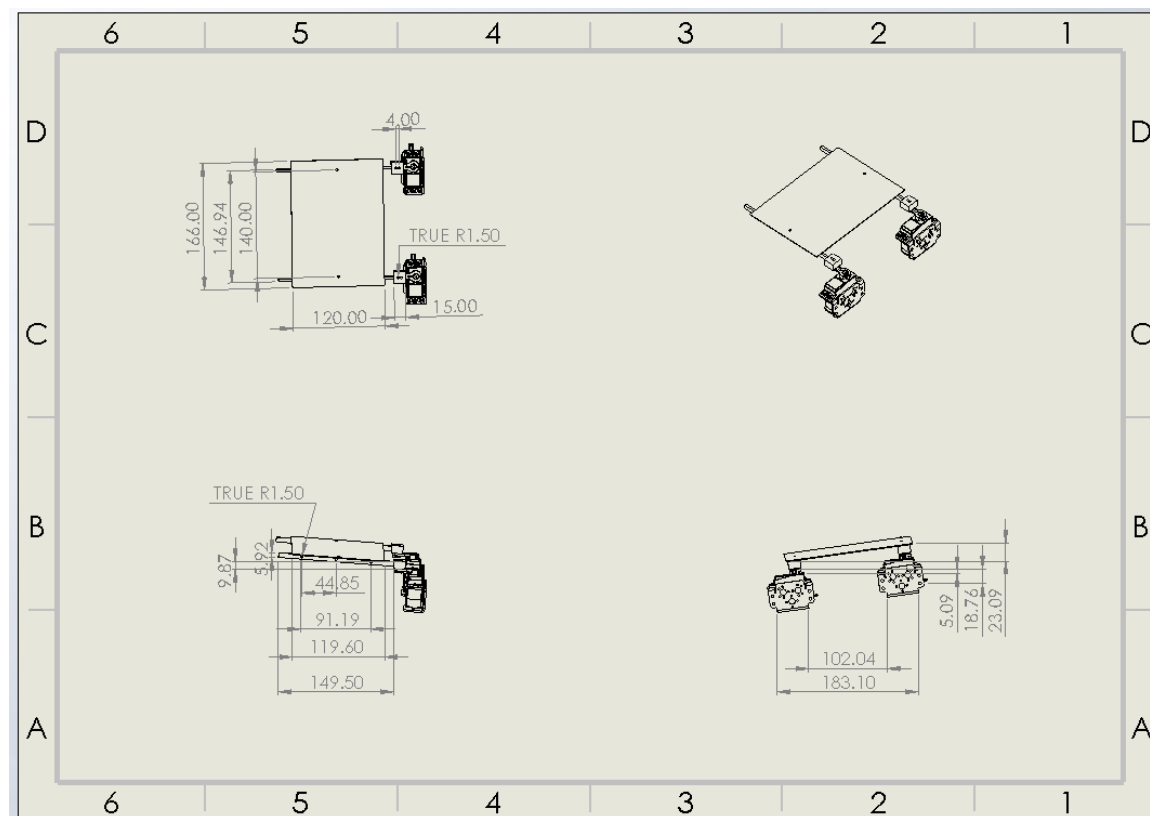
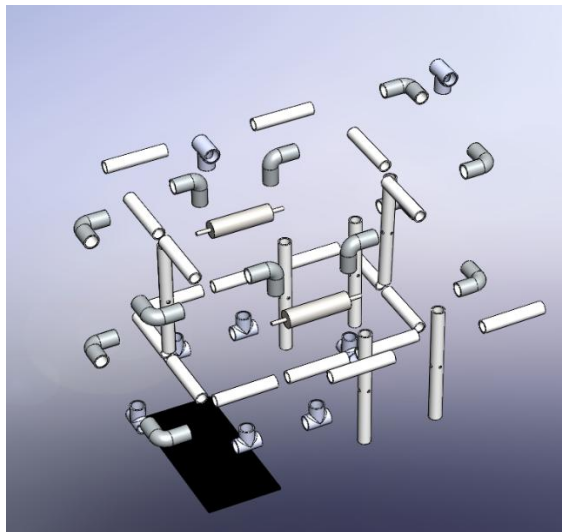


Figure 22: 2D view - Frame

Figure 23: 2D view – *Electronic Enclosure*Figure 24: 2D view – *Thruster-Fin Assembly*

3.5.2 3D CAD Model

Like 2D drawings, three sub-assemblies with exploded parts, 3D view and respective bill of materials are exhibited together.



ITEM NO.	PART NUMBER	QTY.
1	Mounting Joint	2
2	Base Plate	1
3	L-Joint	12
4	Vertical Pipe	6
5	Horizontal Pipe	18
6	T-Joint	8

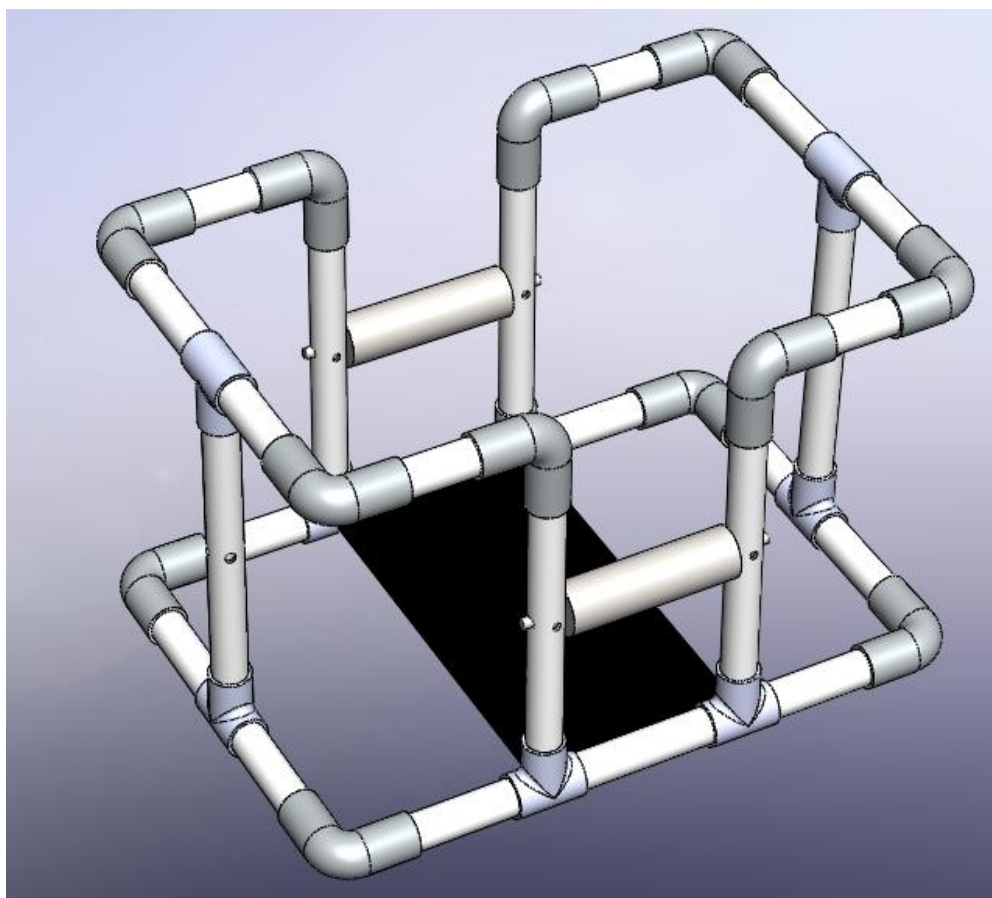
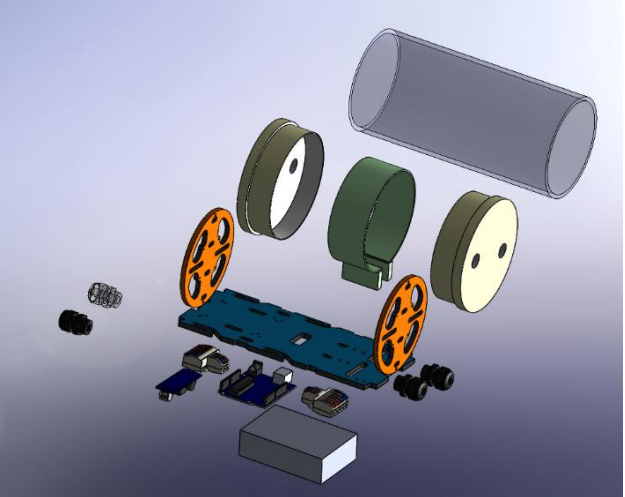


Figure 25: *Exploded view and B.O.M – Frame*



ITEM NO.	PART NUMBER	QTY.
1	2 to 6 Way Connector	2
2	4 inch Pipe	1
3	Arduino Uno	1
4	Cable Gland	4
5	Clamp	1
6	End Cap	2
7	Tray	1
8	Tray Holder	2
9	Voltage Regulator	1
10	SLA Battery	1

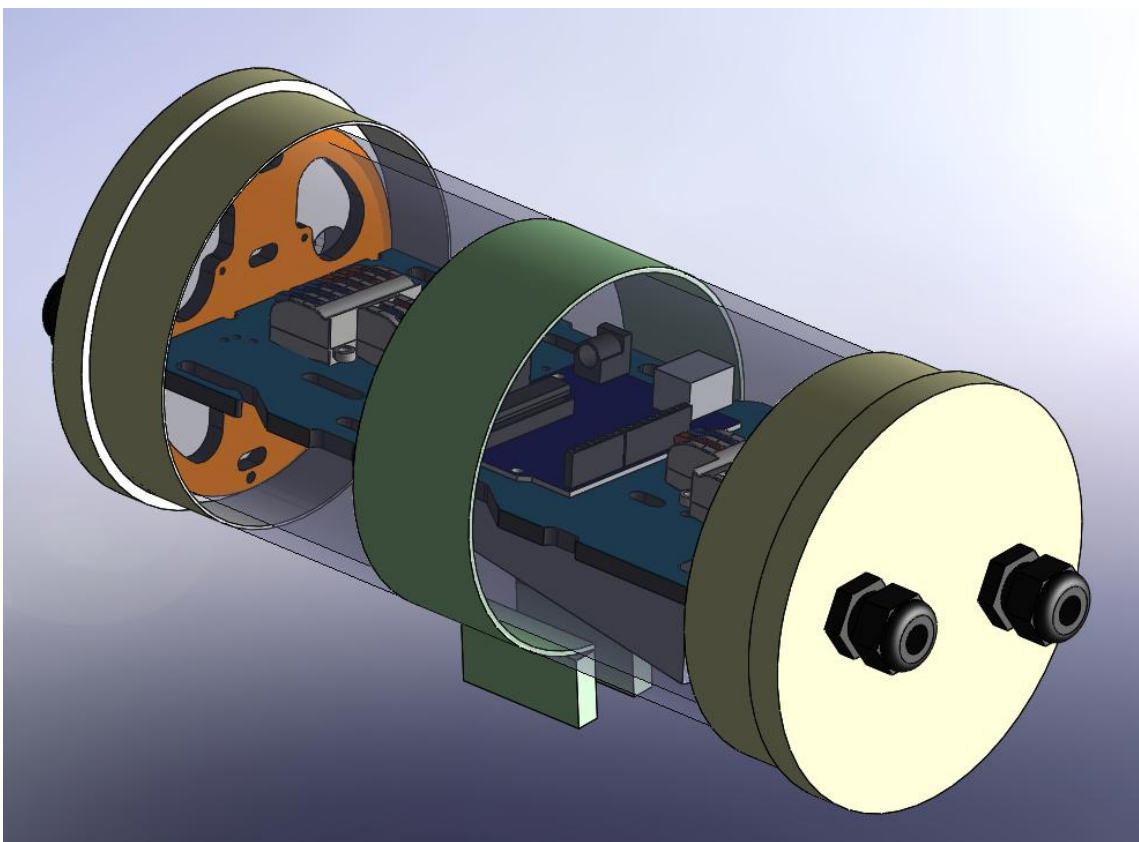
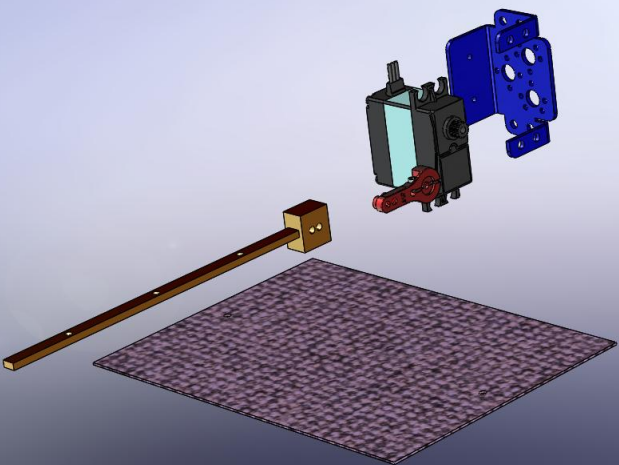


Figure 26: Exploded view and B.O.M – Electronic enclosure

In a thruster system, four sets of following exploded parts and two flexible sheets are contained; two per each side of the frame.



ITEM NO.	PART NUMBER	QTY.
1	Bracket	1
2	Fin	1
3	Servo Horn 25T	1
5	Waterproof Servo	1
6	Rubber Sheet	1

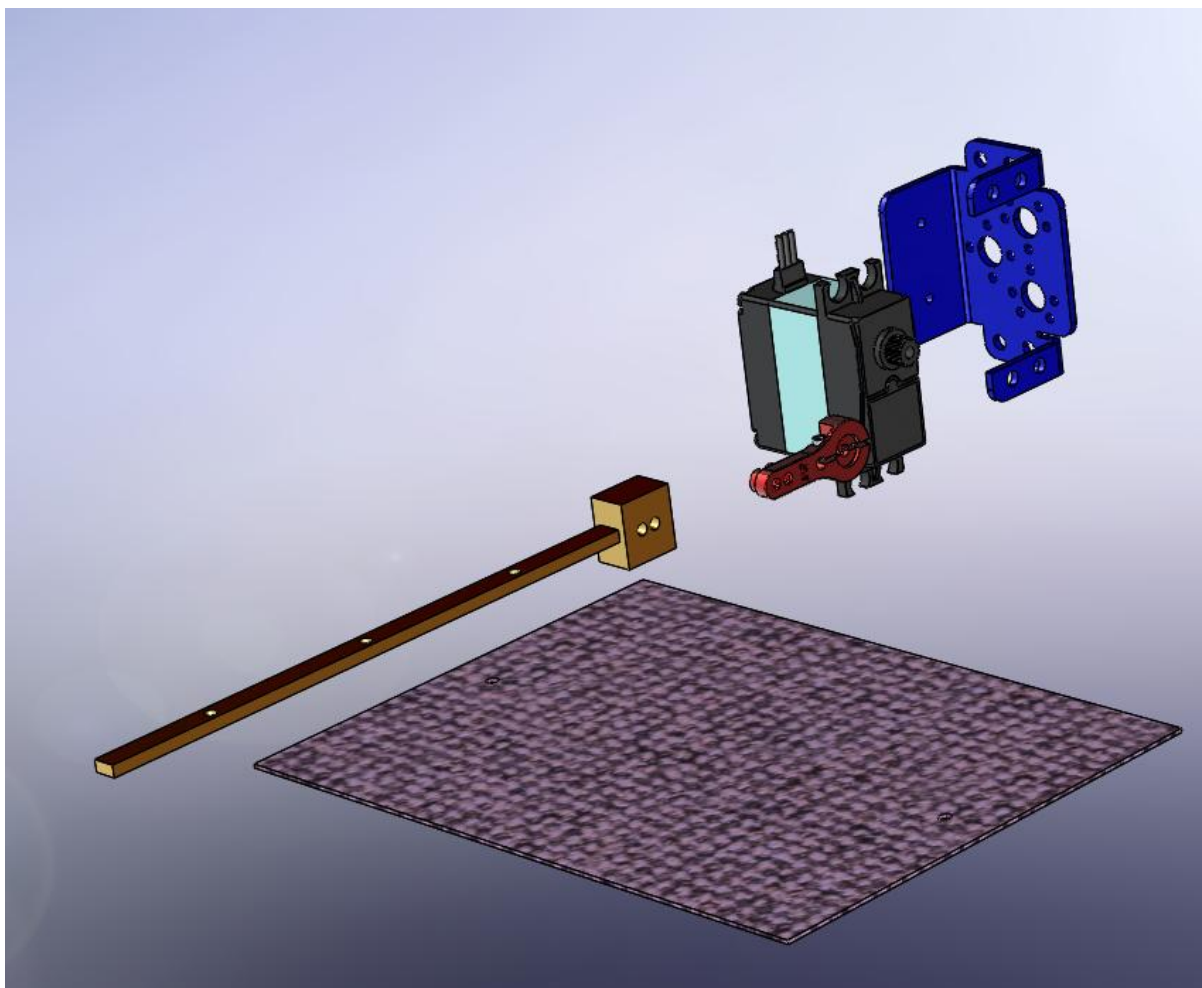


Figure 27: Exploded view and B.O.M – Thruster

The full functional working assembly is shown in Figure 28.

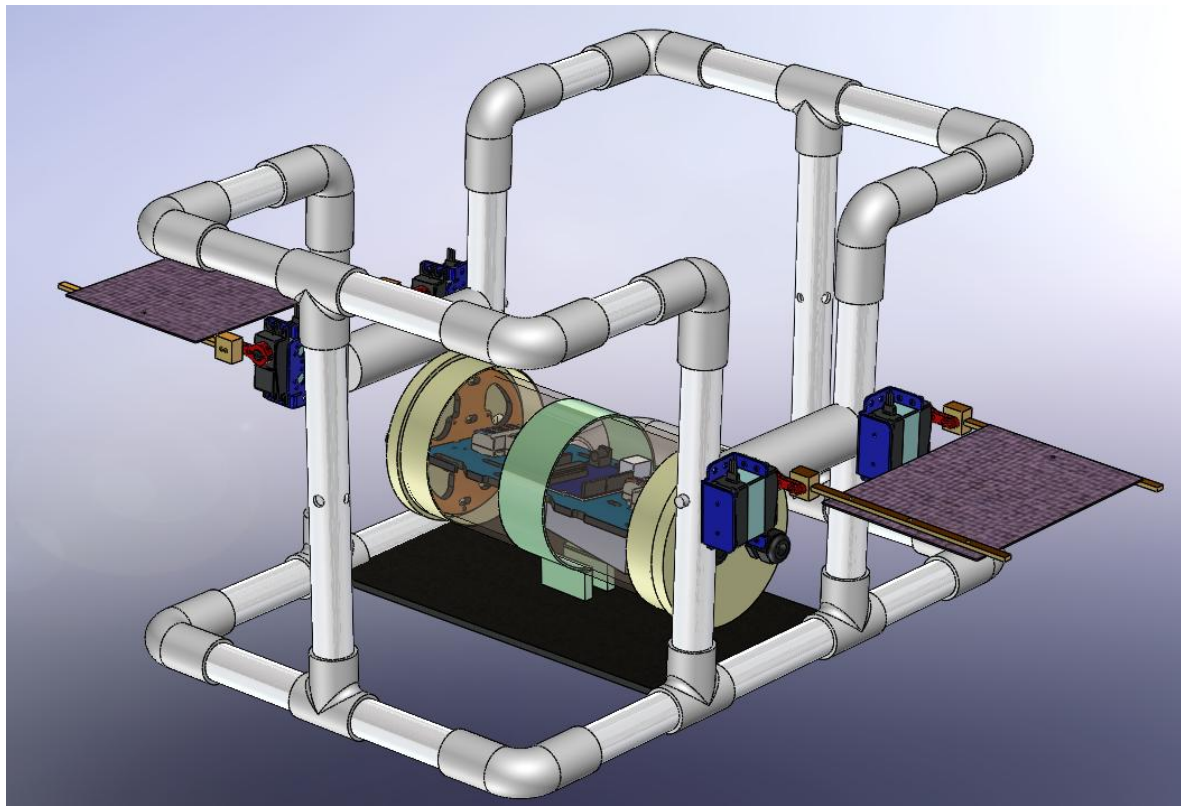


Figure 28: *Full CAD Assembly*

3.6 Design Functionality

Design functionality is a critical aspect of engineering analysis. After modelling the assembly, it is ensured to meet desired performance and operational requirements. This section systematically outlines functionality analysis techniques, such as Function Analysis System Technique (FAST) and Design for Manufacturing and Assembly (DFMA). After that, associated risks of the design are identified with Failure Modes and Effects Analysis (FMEA).

3.6.1 FAST Diagram

A Function Analysis System Technique (FAST) diagram breaks down the working processes into sequential functions. From the input of transmitting power to manoeuvre and propel the ROV, primary steps and relevant secondary functions are related with “How” and “Why”. The following FAST diagram illustrates and summarizes every functional aspect of the thruster system.

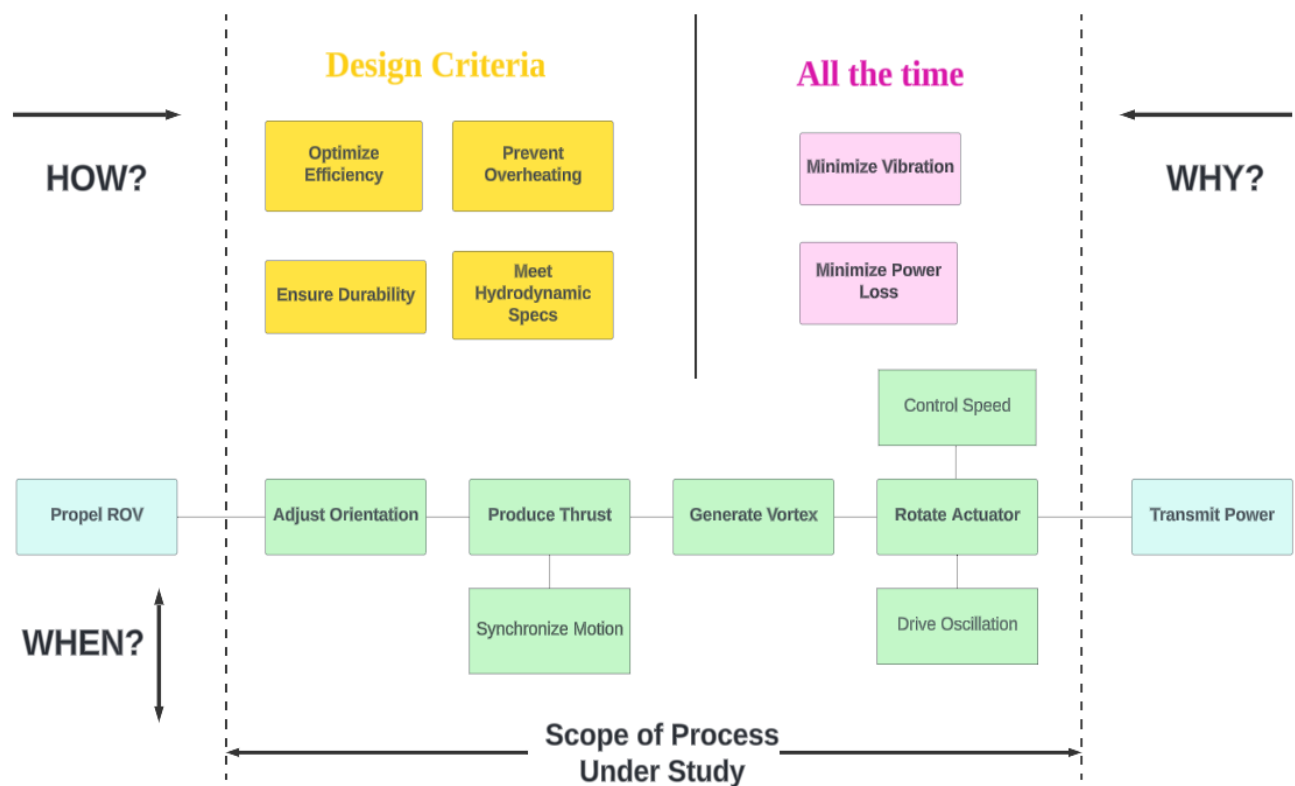


Figure 29: *FAST chart*

3.6.2 Design for Manufacture and Assembly (DFMA)

DFMA is a systematic approach to improve the efficiency of manufacturing and assembly of a product while reducing overall costs. Design for manufacture emphasizes the component fabrication process where material waste is minimized. Design for assembly focuses on ease of assembly and standardizing components. In bio-inspired thruster design, DFMA tool ensures that sub-assembly of thruster components are manufactured and handled cost-effectively. One full set – assembly of fin is analysed here. Depending on amount of fin sets used, the values can multiply accordingly. The analysed components are depicted in following figure.

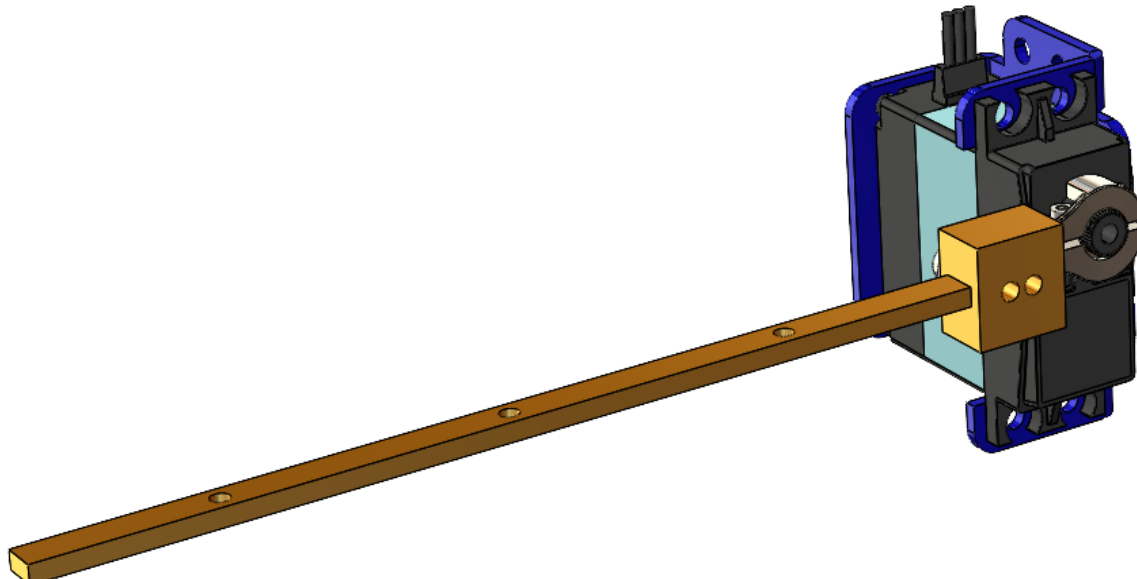


Figure 30: *Thruster system sub-assembly*

Manufacturing cost index (MCI) is calculated first. The values maximize and cover for both versions of fins (printed PLA and aluminium). Formulas and selection steps are in Appendices.

Table 7: MCI Calculation

$$\text{Manufacturing Cost Index} = R_c * P_c + M_c$$

Relative Cost (R_c)

Shape Complexity (Cc)	1.3
Material Suitability (Cmp)	1
Minimum Section (Cs)	1
Tolerance requirement (Ct)	2.2
Surface requirement (Cf)	1.2
$R_c = Cc * Cmp * Cs * Ct * Cf$	3.432

Ideal Process Cost (P_c)	1.2
--	-----

Material Cost (M_c)

Volume of Material (V)	45435.32
Waste Coefficient (Wc)	1.6
Cost of Material (Cmt)	0.00078
$M_c = V * Wc * Cmt$	56.7

Therefore, Manufacturing Cost Index = $R_c * P_c + M_c = 60.81$

For design for assembly part, manual handling index and fitting index are estimated. The handling index measures the difficulty of component connections and the latter determines the difficulty of parts assembly/disassembly. Firstly, all the parts included in fin assembly is differentiated part 'A' or 'B', according to their functions that are critical during operations.

Design efficiency is calculated by dividing numbers of part 'A' to total numbers of part counted. Handling and fitting index are configured with all components included in the fin assembly. The scores are depicted in Table 8.

Table 8: Design for assembly

Components	Quantity	Handling					Handling Index	Fitting						Fitting Index
		A	B	C	D	SUM		A	B	C	D	E	F	
Bracket (A)	1	1.5	0.2	0.5	0.2	2.4	$\frac{\text{Total Sum}}{\text{'A' Parts}}$ = 3.17	2	0	0.7	0	0.7	0	3.4
M3 screws (B)	6	1.5	0	0	0	1.5		1.3	0	0.7	0	0	0	2
Washers (B)	3	1	0	0	0	1		1	0	0.7	0	0	0	1.7
Servo Motor (A)	1	1.5	0.2	0.1	0.2	2		2	0	0	0	0	0	2
Servo Horn (A)	1	1.5	0.2	0.1	0.2	2		2	0	0.7	0	0.7	0	3.4
Horn Fastener (B)	1	1.5	0	0.1	0	1.6		1.3	0	0	0	0	0	1.3
Fin (A)	1	1.5	0.4	0.1	0.2	2.2		4	0	0.7	0	0	0	4.7

As seen in the table, manual handling for each component falls within optimum range. The fitting index is high due to the delicate nature of fin and detailed precision while mounting it. However, the values suggested that the assembly is achievable with proper care. Reducing the number of screws, washers and bolts while using adhesive instead can also lower both scores.

The design efficiency is at 28.6 %. This suggests the effective value for one sub-assembly. Similar to above, reducing the screws will distinctly enhance the overall efficiency.

3.6.3 Failure Mode and Effect Analysis (FMEA)

To identify, assess, and mitigate potential failures within the system, FMEA approach is carried out. This is crucial for current design because operational failures can lead to significant performance losses or even mission failure. By analysing failures before prototype and designing stage, Risk Priority Number (RPN) is known beforehand and solutions to reduce it can be determined. The following section focuses on key areas such as motor malfunction, water leakage into electronics enclosure, and structural integrity due to buoyancy. RPN is achieved by multiplying SEV (severity), OCC (occurrence), and DET (detection).

Table 9: *FMEA Table*

Function / Process	Failure Type	Potential Impact	SEV	Potential Cause	OCC	Detection Mode	DET	RPN
Fin Oscillation (Thruster System)	Servo motor failure	Loss of propulsion, uneven thrust	8	Motor overheating, mechanical wear, incorrect synchronization	6	Irregular fin motion, abnormal noise, response delay	5	240
Electronics Housing	Water ingress	Complete electronics failure, ROV shutdown	9	Poor sealing, cracked housing, worn-out O-rings	7	System shutdown, erratic sensor readings	5	315
Buoyancy System	Structural instability	Imbalanced movement, difficulty maintaining depth	7	Weak joints, frame deformation, broken fastener linkage	5	Unstable motion, unusual vibrations	4	140

Each process and failure type are expected to reduce RPN by proposing respective solutions. Severity rate cannot be reduced but occurrence rate and detection mode can be enhanced. Responsible parties and target dates to take actions are also presented. The new results are depicted in following table.

Table 10: *Solution Table*

Recommended Action	Responsibility	Target Date	Action Taken	SEV	New OCC	New DET	New RPN
Implement redundant motor control system with real-time feedback	R&D Team	From immediate effect	Installed backup servo system and PID controller	8	4	3	96
Use high-quality silicone O-rings and dual-layer sealing	Design Engineer	From immediate effect	New seals tested in high-pressure conditions	9	4	3	108
Reinforce frame with carbon fiber or aluminum joints and optimize buoyancy	Mechanical Team	From immediate effect	Reinforcement added, stability test passed	7	3	3	63

By implementing the controlled actions, the risk values are significantly decreased. To design a full functional model, reliability and durability are identified before moving onto simulations and prototyping.

3.7 Preliminary Analysis of Stress and Hydrodynamic Loads

Before assembling the prototype or developing a product, the model must undergo simulations in order to meet certain design limitations and expected performance outcomes. Finite element analysis is run to evaluate the structural integrity of the design, whereas computational fluid dynamics is conducted to assess the fluid interactions around it. The results will be discussed in next chapter.

3.7.1 Finite Element Analysis (FEA) Simulation

FEA tests the component strengths under applied loads at real world scenario. This is to ensure how the selected materials and mating procedures can withstand under operational behaviours. Von Mises's stress and relevant strain will be analysed together with equivalent displacement.

The main loads acting on ROV under certain depth include: downward gravitational force at the base of the frame, upward buoyant force at the centre of submerged volume, water pressure around every single part, horizontal thrust force in the direction of forward motion generated by motor to the fin, and opposing drag force in reverse that is proportional to the velocity of ROV. Base plate is fixed reference and vertical pipes act as roller/sliding constraints to allow freedom of motion. Meshed body with boundary conditions for whole assembly is as below.

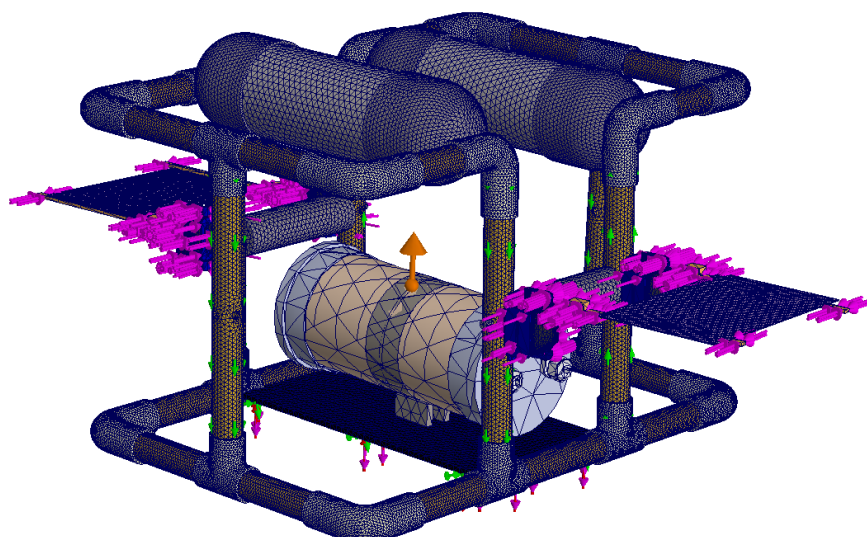


Figure 31: *Meshed body with boundary conditions*

In order to achieve the specific results for thruster, the fin-motor sub-assembly is extracted from the whole frame. One side of thruster set is simulated for prototype testing conditions in a pool. The values are estimated at 2 meters water depth and 0.5 m/s velocity. Given boundary conditions are stated and visualized in following table and figure.

Table 11: FEA pre-processing values

Boundary Condition	Component	Fixture Details
Fixtures	Brackets	Entities: 2 face(s) Type: Fixed Geometry
Hydrodynamic Pressure ($P=\rho \cdot g \cdot h$)	Sheet and Fins	Entities: 19 face(s) Type: Normal to selected face Value: 6,500 Units: N/m ² Phase Angle: 0 Units: deg
Drag Force ($F_d=1/2 \cdot \rho \cdot C_d \cdot A \cdot v^2$)	Horns and Fins	Entities: 12 face(s) Type: Apply normal force Value: 5 N
Thrust Force ($F_t=\rho \cdot C_t \cdot A \cdot v^2$)	Horns and Fins	Entities: 15 face(s) Type: Apply normal force Value: 8.3 N

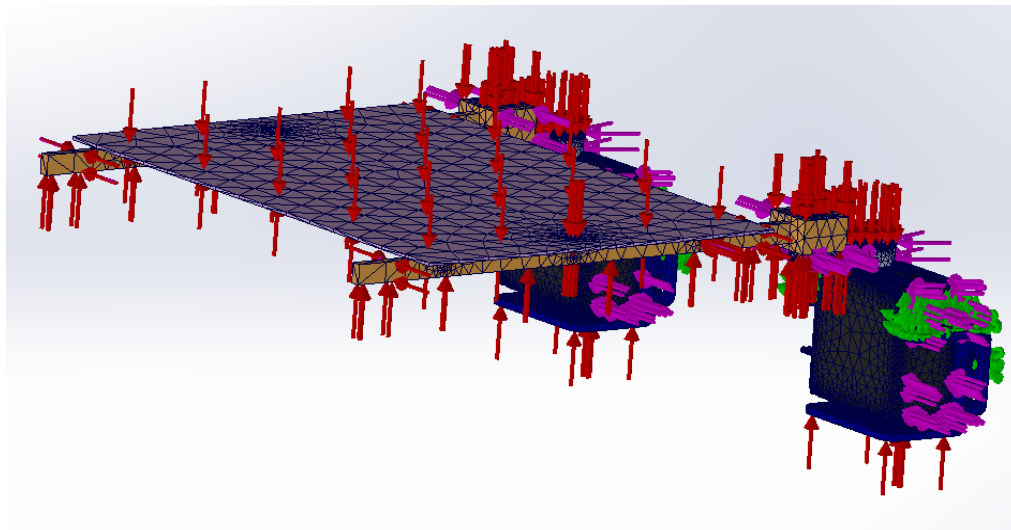


Figure 32: FEA pre-processing conditions

3.7.2 Computational Fluid Dynamics (CFD) Simulation

Fluid flow around thrusters is simulated in CFD analysis. This is done to analyse hydrodynamic behaviour of bio-inspired thruster. Factors such as thrust generation, drag forces, pressure distribution, and fluid flow characteristics are assessed. This study focuses on understanding flow separation, vortex formation, pressure distribution, and force generation by the fins. By validating these parameters, design can enhance manoeuvrability and efficiency before physical prototyping. Boundary conditions are as follows.

Table 12: *CFD pre-processing parameters*

Parameter	Description
Flow Type	Turbulent (k- ϵ model)
Fluid Medium	Water (Density: 997 kg/m ³ , Viscosity: 0.001 Pa·s)
Computational Domain	Box around thruster (External Flow)
Velocity Inlet	~ 0.5 – 1.5 m/s
Pressure Outlet	0 Pa (Gauge Pressure)
Boundary Layer	Automatic/ Inflation Layer
Gravity Effect	9.81 m/s ² (-Z direction)
Time Model	Steady-State (basic motion) / Transient (dynamic study)
Cavitation	Off (moderate velocity)
Turbulence Parameters	Intensity ~5%, Length Scale ~0.01 m

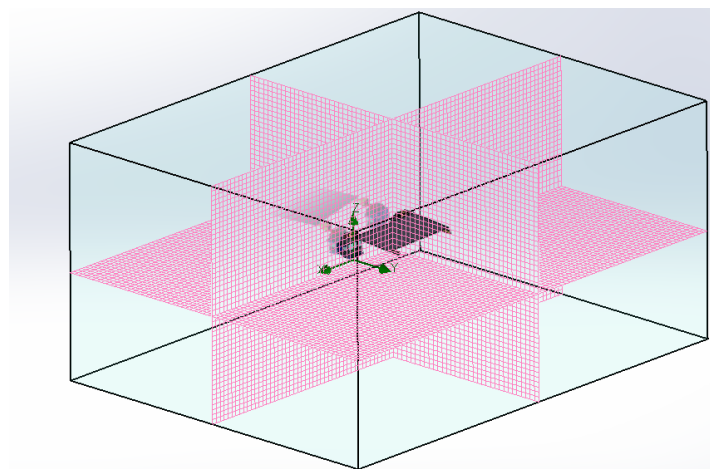
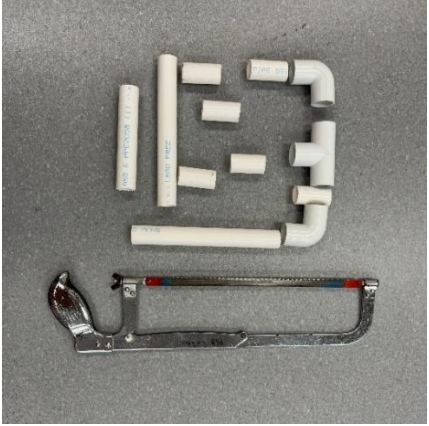


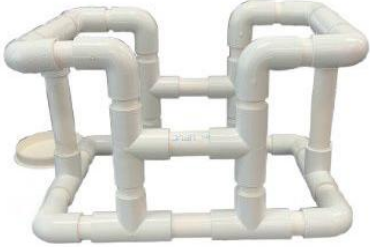
Figure 33: *Meshed model inside water domain*

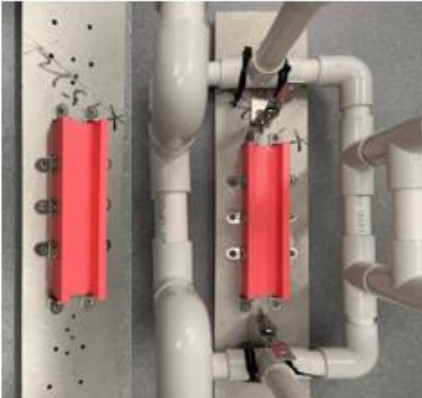
3.8 Prototyping

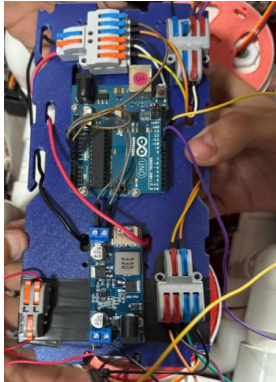
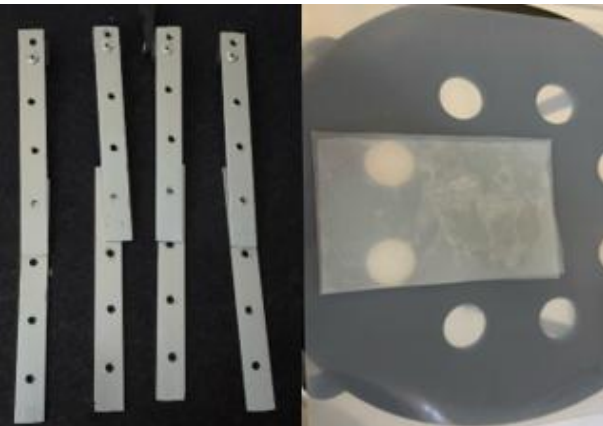
3.8.1 Process of Fabrication

Table 13: *Fabrication Steps*

Step	Description
	<p>Pipe segments and the joints (T joints and elbow joints) are cut as required dimensions; 5 cm for horizontal pipes and 10 cm for vertical pipes.</p>
	<p>All the segments are then cleaned with dry cloth. By using PVC primer and PVC cement, pipes and joints are connected firmly with care.</p>
	<p>Sharp edges are smoothed with file for better securement.</p>

	<p>Final frame assembly is achieved with exact dimensions. Proper grid and strength are needed so that other sub-components can be attached by force as required.</p>
	<p>The sides shafts are marked with chisel and drilled for servo motor brackets. Since the surfaces of the pipes are smooth, extensive care and assistance are necessary.</p>
	<p>Base holder for electronic enclosure is drilled and joined with small metal brackets. The inner channel is also used for ballast placement.</p>

	<p>The holder is placed at center on the aluminum base plate. The plate is then joined with the frame vertically with the cable ties firmly.</p>
	<p>For the enclosure ends, 4" PVC cap is used. It is drilled with 15" bit so that PG-9 cable glands can be inserted. Since the cap is soft and machine speed is fast, the former can spin out from the place. Full PPEs and firm gripper are recommended.</p>
 	<p>Inside the enclosure, tray and a set of holder wheels are used for electronics placement. They are 3D printed, and the holes must allow in-and-out wires and screws.</p>

	<p>Circuit boards, voltage regulators and Arduino are placed upside of the tray and batteries are placed below. Wires are secured with block connectors and joined through the grooves. Every connection must be firmly fixed before placing inside the enclosure. One loose wire could halt the whole process.</p>
	<p>For the fin hands, 1 mm aluminum sheet is cut at specific length and drilled three holes at 2.5 cm apart.</p>
	<p>Four sets of fins are to be connected later with flexible silicon sheet. Two identically cut rubbers are sticked together with glue.</p>
	<p>Blockhead horn which will be connected to servo arm, aluminum sheets, and sticked rubber sheets are all riveted together because they can be loosen up underwater.</p>

 A photograph showing two black servo brackets mounted on white PVC pipes. The brackets are secured with black zip ties and are positioned on pre-drilled joints of the pipe system.	<p>Servo brackets are then mounted on the pre-drilled joints.</p>
 A photograph showing a close-up of a white metal bracket. Inside the bracket, there are two black servo motors labeled "DS18MG-180" and "DS18MG-180". Wires from the servos are visible, and the bracket is being held by a hand.	<p>Combined lateral attachment is finally placed inside the bracket and screwed along.</p>
 A photograph showing a close-up of a white cylindrical pipe. A black servo motor is attached to the pipe, and its wires are being inserted through a cable gland. The pipe has markings "PPE20" and "15 E".	<p>Servo and battery wires are inserted together into the enclosure pipe through cable glands. Rubber seals are additionally coated with silicone gel for external waterproofing.</p>

3.8.2 Final Assembly

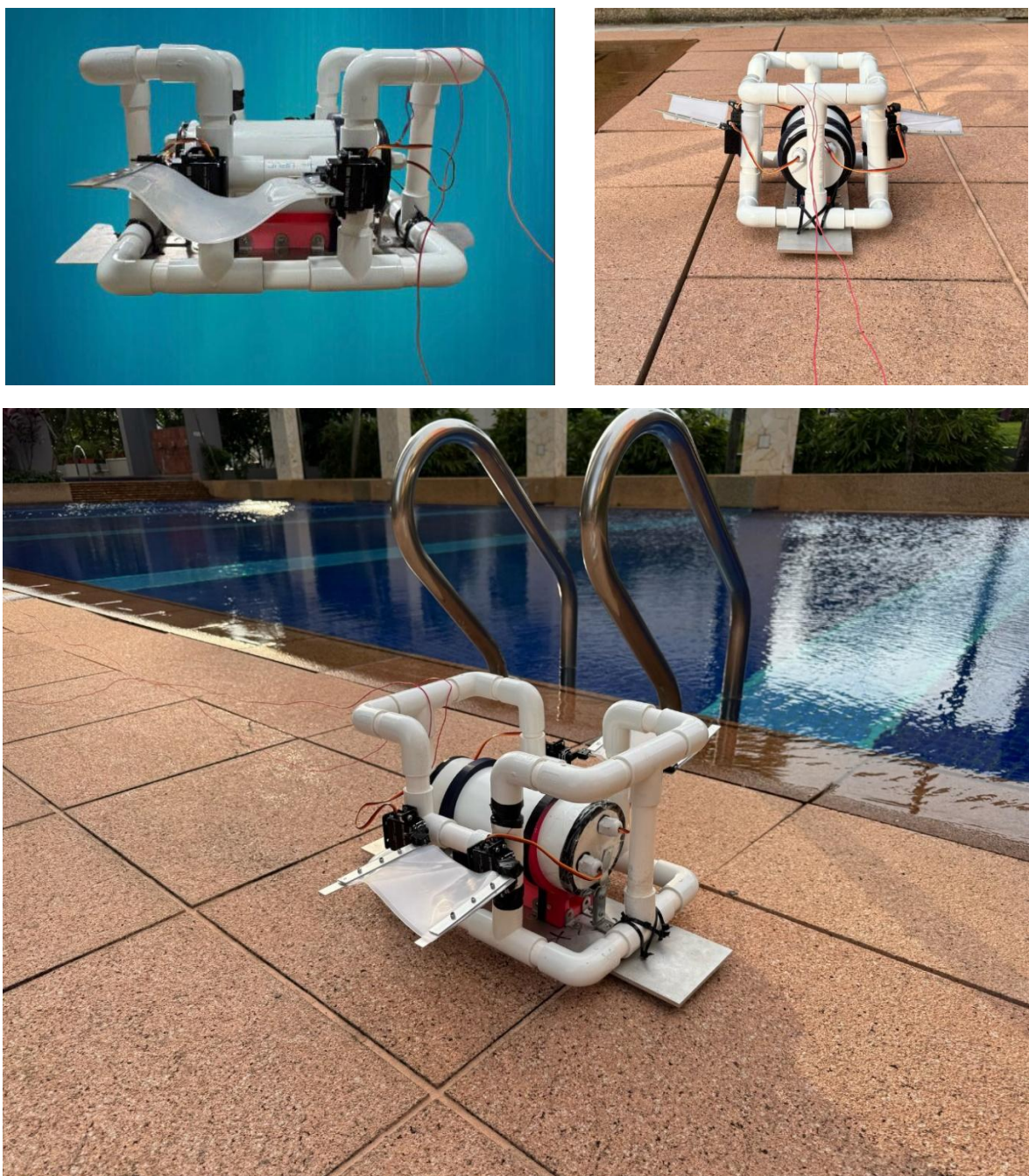


Figure 34: Side view, front view and isometric view of prototype

3.8.3 Control Algorithm

The control algorithm governing the undulating propulsion of ROV is described in this section. The algorithm is divided into modular functions that allow precise control over key parameters. These include: flapping frequency, amplitude, and duration for different phases of the mission (forward motion, turning, and return).

```
1 #include <Servo.h>
2
3 // Servo objects for each fin
4 Servo rightFrontFin, rightBackFin;
5 Servo leftFrontFin, leftBackFin;
6
7 // Neutral PWM value corresponding to 180° (horizontally outward)
8 const int NEUTRAL = 1500;
9
10 // Default amplitude in microseconds (controls fin deflection)
11 // ±400 corresponds approximately to a range of 90°–270° for extended servos.
12 int amplitudeForward = 400;
13 int amplitudeTurnLeftFront = 600; // Stronger left side for turning
14 int amplitudeTurnRight = 50; // Weaker right side during turn
15
16 // Phase offsets (in degrees) for undulation between fins
17 const int phaseRightBack = 90;
18 const int phaseLeftFront = 180;
19 const int phaseLeftBack = 270;
20
21 // Timing parameters
22 // "stepDelay" determines how long each step lasts (ms), affecting frequency.
23 // "stepAngle" is the step increment in degrees for the sine wave.
24 int stepDelay = 20;
25 int stepAngle = 10;
26
27 // Forward and turn durations (ms)
28 unsigned long durationForward1 = 120000; // 2 minutes
29 unsigned long durationTurnLeft = 4000; // 4 seconds
30 unsigned long durationForward2 = 180000; // 3 minutes
31
32 // Function to execute one full cycle of flapping motion
33 // "ampRF", "ampRB", "ampLF", "ampLB" define the amplitude for each fin
34 // "phaseOffsetRF", etc., allow fine-tuning individual fin phases if needed
35 // "cycleSteps" defines resolution of the sine wave
```

```

36 void runCycle(int ampRF, int ampRB, int ampLF, int ampLB,
37             |           |           |           |           |
38             |           int phaseOffsetRF, int phaseOffsetRB, int phaseOffsetLF, int phaseOffsetLB,
39             |           |           |           |           |
39     for (int t = 0; t <= 360; t += cycleSteps) {
40         int pwmRF = NEUTRAL + ampRF * sin(radians(t + phaseOffsetRF));
41         int pwmRB = NEUTRAL + ampRB * sin(radians(t + phaseOffsetRB));
42         int pwmLF = NEUTRAL + ampLF * sin(radians(t + phaseOffsetLF));
43         int pwmLB = NEUTRAL + ampLB * sin(radians(t + phaseOffsetLB));
44
45         rightFrontFin.writeMicroseconds(pwmRF);
46         rightBackFin.writeMicroseconds(pwmRB);
47         leftFrontFin.writeMicroseconds(pwmLF);
48         leftBackFin.writeMicroseconds(pwmLB);
49
50         delay(stepDelay);
51     }
52 }
53
54 // Function to run a behavior for a given duration (in ms)
55 // "ampRF", etc., and phase offsets are passed to runCycle repeatedly.
56 void runBehavior(unsigned long durationMillis,
57                  |           |           |           |           |
58                  |           int ampRF, int ampRB, int ampLF, int ampLB,
59                  |           |           |           |           |
59     unsigned long startTime = millis();
60     while (millis() - startTime < durationMillis) {
61         runCycle(ampRF, ampRB, ampLF, ampLB, phaseOffsetRF, phaseOffsetRB, phaseOffsetLF, phaseOffsetLB, stepAngle);
62     }
63 }
64
65 void setup() {
66     // Attach servos to chosen PWM pins.
67
67     rightFrontFin.attach(3);
68     rightBackFin.attach(10);
69     leftFrontFin.attach(11);
70     leftBackFin.attach(12);
71
72     // Initialize all fins to the neutral position.
73     rightFrontFin.writeMicroseconds(NEUTRAL);
74     rightBackFin.writeMicroseconds(NEUTRAL);
75     leftFrontFin.writeMicroseconds(NEUTRAL);
76     leftBackFin.writeMicroseconds(NEUTRAL);
77
78     delay(1000); // Allow servos to stabilize.
79 }
80
81 void loop() {
82     // Phase 1: Forward Motion for 2 minutes using full amplitude on all fins.
83     runBehavior(durationForward1,
84                 |           |           |           |           |
84                 |           amplitudeForward, amplitudeForward, amplitudeForward, amplitudeForward,
85                 |           |           |           |           |
85                 |           0, phaseRightBack, phaseLeftFront, phaseLeftBack);
86
87     // Phase 2: Turn Left for 4 seconds.
88     // In this maneuver, reduce the right fin amplitude (weaker thrust)
89     // while keeping the left fins at full amplitude, causing a left turn.
90     runBehavior(durationTurnLeft,
91                 |           |           |           |           |
91                 |           amplitudeTurnRight, amplitudeTurnRight, amplitudeTurnLeftFront, amplitudeTurnLeftFront,
92                 |           |           |           |           |
92                 |           0, phaseRightBack, phaseLeftFront, phaseLeftBack);
93
94     // Phase 3: Forward Motion (Return) for 3 minutes, using full amplitude.
95     runBehavior(durationForward2,
96                 |           |           |           |           |
96                 |           amplitudeForward, amplitudeForward, amplitudeForward, amplitudeForward,
97                 |           |           |           |           |
97                 |           0, phaseRightBack, phaseLeftFront, phaseLeftBack);
98
99     // Stop all movement.
100
100    rightFrontFin.writeMicroseconds(NEUTRAL);
101    rightBackFin.writeMicroseconds(NEUTRAL);
102    leftFrontFin.writeMicroseconds(NEUTRAL);
103    leftBackFin.writeMicroseconds(NEUTRAL);
104    while (true); // End of sequence.
105 }

```

Figure 35: *Arduino code for motion*

Parameters can be adjusted by changing the function values as follows.

Flapping frequency – A smaller `stepDelay` or `stepAngle` increases the number of cycles per second. Reducing `stepDelay` from 20 ms to 10 ms will roughly double the flapping frequency.

Amplitude – Changing `amplitudeForward` affects how far the fins deflect during forward motion. A higher amplitude produces a larger fin swing, displacing more water and generating more thrust. During turning, altering `amplitudeTurnRight` and `amplitudeTurnLeftFront` changes the asymmetry between sides and controls the turning rate.

Timeframe – Duration of each motion phase is set by the corresponding duration variables. This modularity allows to modify the mission timing without altering the core motion algorithms.

4. Result and Discussion

This chapter compares and discusses the results between simulations and prototype experiment. The outcomes are then validated and integration towards ROV framework is discussed.

4.1 Simulation Results

4.1.1 FEA Outcomes

In stress distribution result, great value of stress is concentrated on the face of servo horn with the value of 19 MPa, shown in green colour. This is because it is the motion transmission point from servo to fin. The value is well within safe limits of material's yield strength and should be structurally sound in upcoming prototype. Rubber sheet and PLA joint blocks experienced relatively low stress of 6 MPa. This indicates good flexibility under loading. Fin tips and edges are all blue regions, indicating the durability of the design.

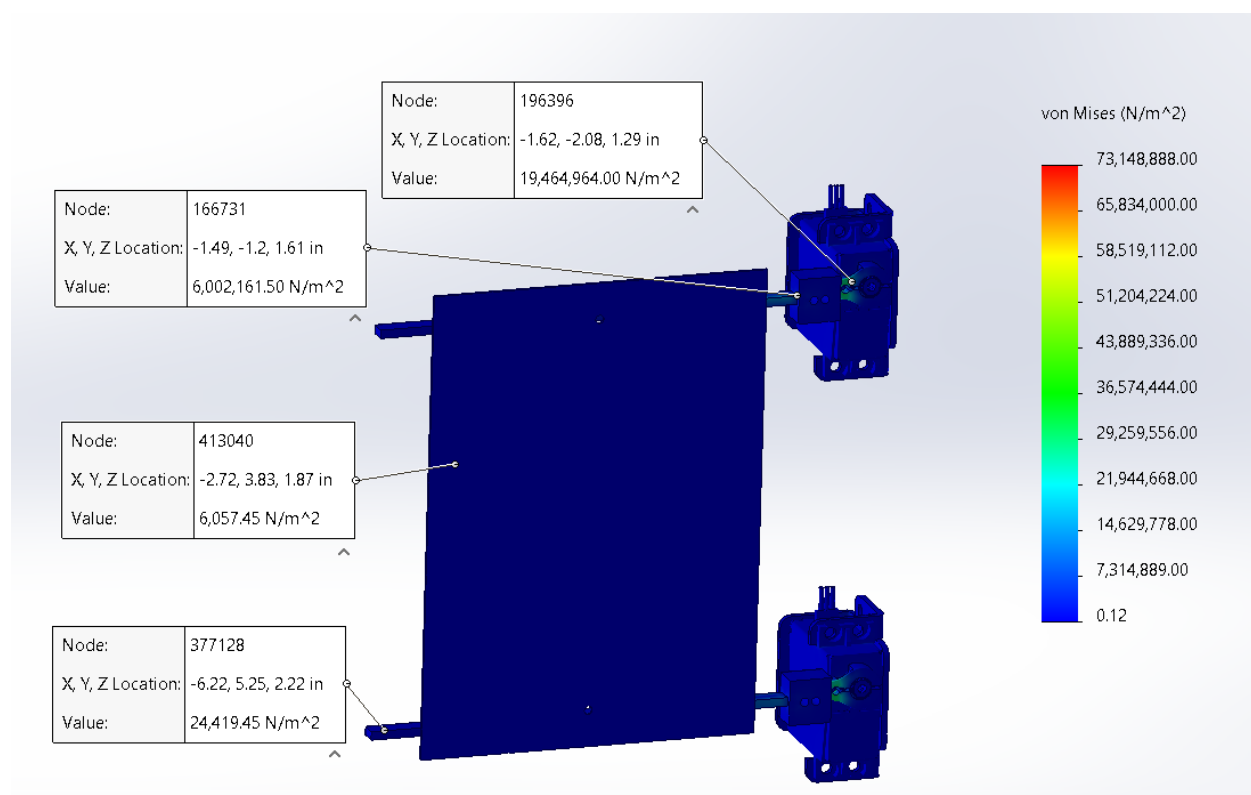


Figure 36: Von Mises stress

Maximum displacement is seen at the far tip of the fin. Since the value is just under 1 mm, the slight movement can be negligible. However, repeated run under water might alter displacement due to added hydrodynamic forces. Nevertheless, it should remain minimal unless material deforms overtime. Flexible sheet's displacement 0.4 mm confirms that the rubber absorbs stress without excessive stretching. The connecting block also remains rigid with the value of 0.035 mm. This means servo torque is effectively transmitted with minimal flex.

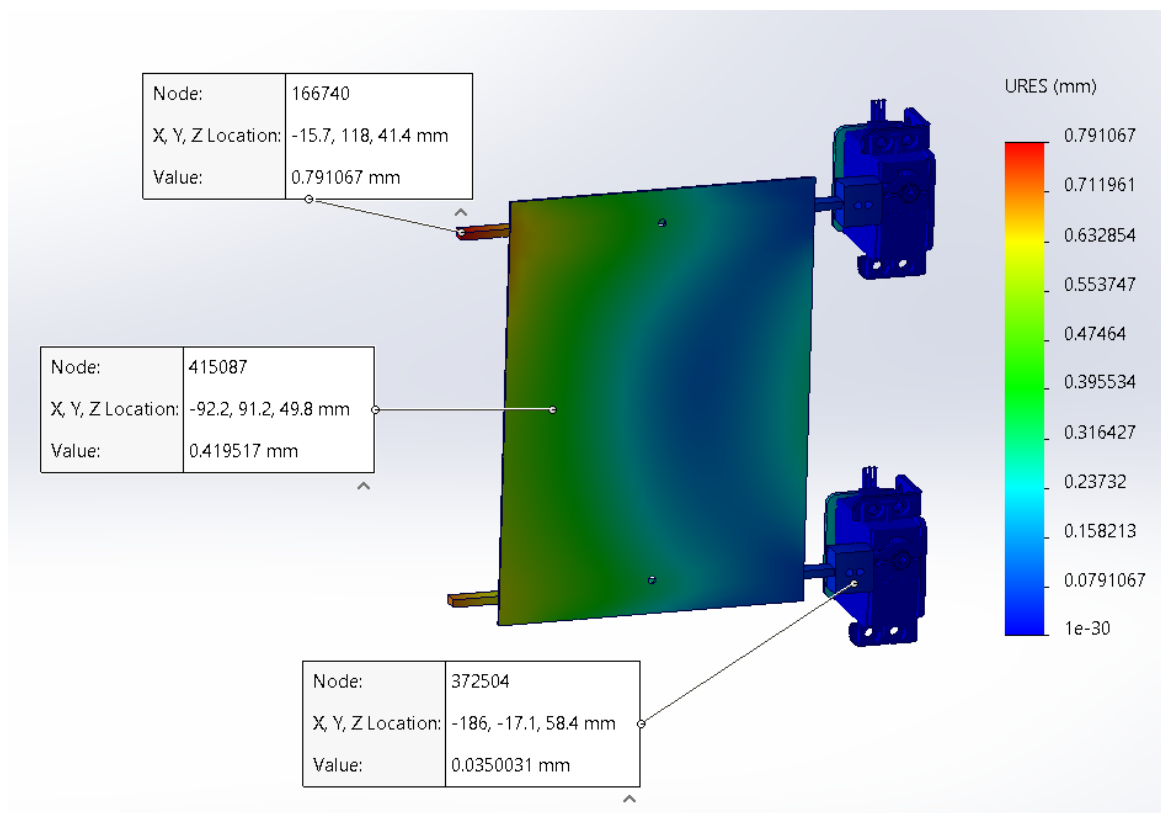


Figure 37: Resultant Displacement

Respective equivalent strain is seen along the edges of the sheet. Rubber materials typically handle strains up to ~0.6 (60%) before failure (Zhu & Li, 2021), so 0.007 (0.7%) is very safe and sustainable.

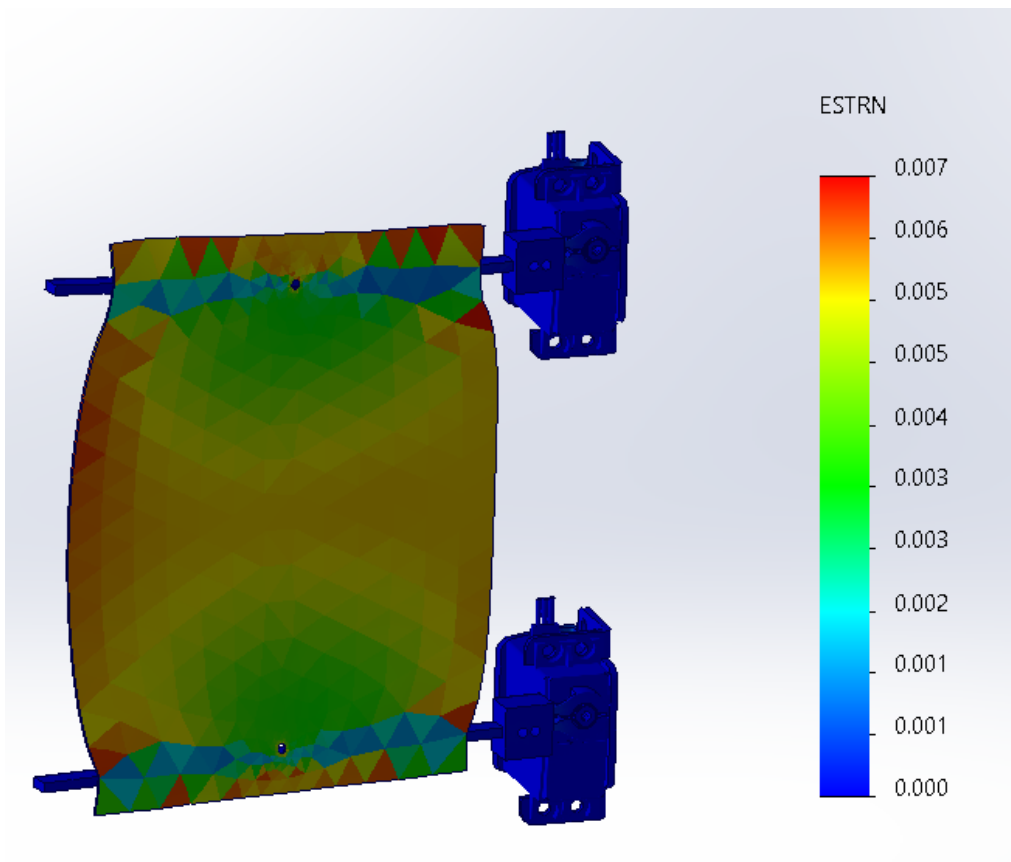


Figure 38: *Equivalent strain*

4.1.2 CFD Outcomes

Pressure contours and isolines suggest the pressure distribution around thruster assembly. The overall pressure ranges between 94486 Pa to 105534 Pa. This means that the thruster operates within typical hydrodynamic environment. Observed differential pressure and wake regions contribute to lift and thrust generation. This validates the oscillatory motion due to fins.

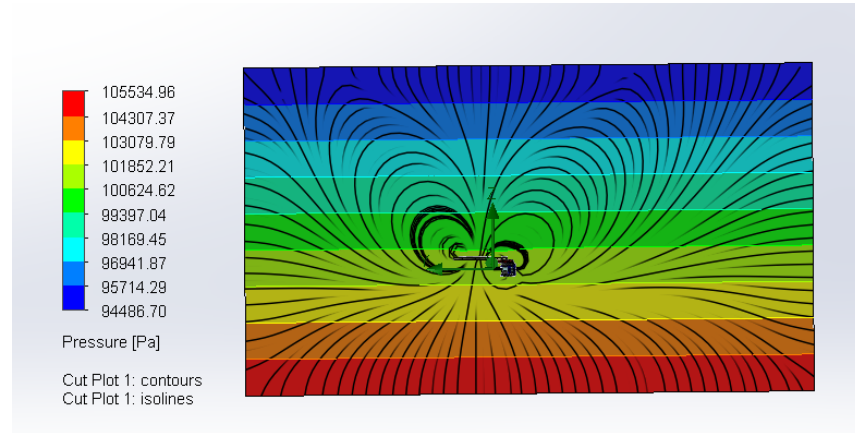


Figure 39: Pressure plot

Velocity plot (Figure 40) provides the pattern of flow behavior. The highest velocity (red color) is 1.72 m/s. This occurs definitely around tilting fins, indicating that they are displacing fluids effectively. The flow field shows symmetrical patterns with smooth velocity gradient. Gradual velocity decay occurs with wake regions behind the thruster. This indicates that thruster does not introduce excessive energy dissipation. This velocity distribution supports the expected sinusoidal motion and confirms that the oscillatory thruster is effectively interacting with the fluid.

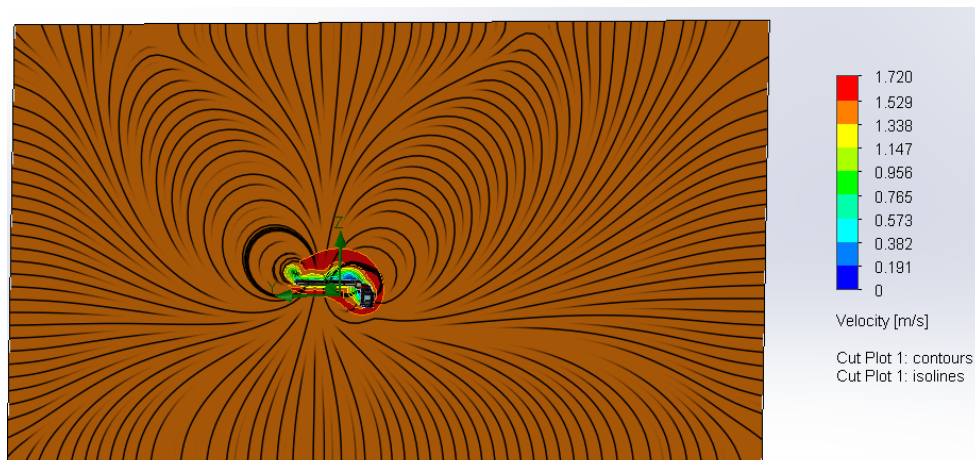


Figure 40: Velocity plot

Vorticity plot (Figure 41) illustrates the rotational flow around the fins. High vorticity ($\sim 2047 \text{ 1/s}$) is observed along the fin edges. The wake region extends behind the thruster but the vortex shedding is consistent. This suggests the stable thrust production mechanism. The presence of these organized vortex supports the thruster's ability to produce net forward thrust.

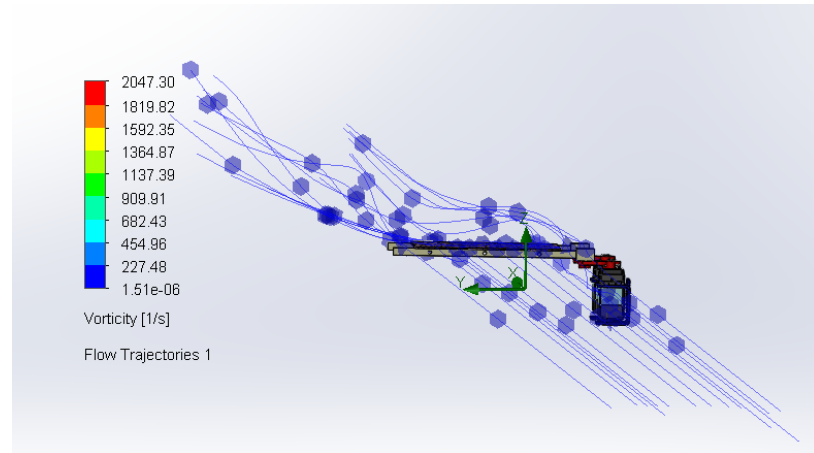


Figure 41: Vorticity plot

Shear stress is studied on the exposed faces of the flexible rubber sheet. Maximum shear stress peaks at 5 Pa and average value stabilizes at 3.3 Pa. Even the maximum value is significantly lower than the material's failure limit and thus, the sheet should withstand repeated oscillation without immediate damage. However, hydrodynamic fatigue effects, cyclic loads, and additional abrasive forces that may present in deeper ocean floor could lead to micro-tearing and degradation overtime.

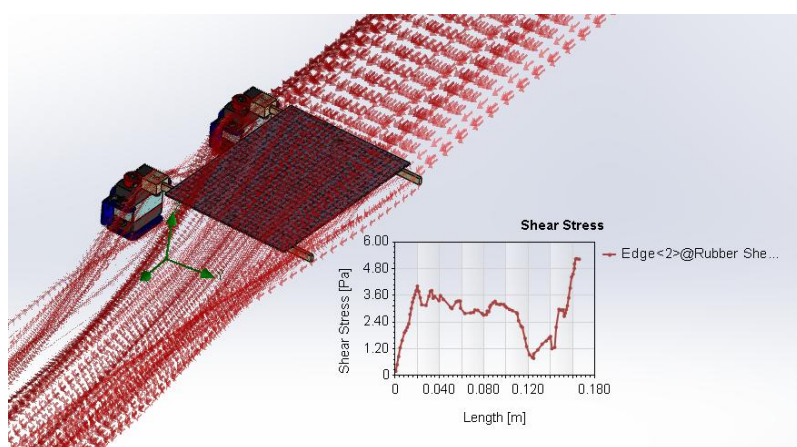


Figure 42: Flowline plot with shear stress

The goal graph is shown in following figure. Maximum static and dynamic pressure are converged after 201 iterations at 105,407 Pa and 1743 Pa respectively. The forward thrust force acting on one set of thrusters is averaged at 4.57 N. Total combined value of net force for both sides can be estimated around 10 N, which lies in reasonable range for small-scale ROV.

Name	Current Value	Progress	Criterion	Averaged Value
GG Force (X) 3	4.58236 N	Achieved IT > 201	0.207439 N	4.57521 N
GG Maximum Dynamic Pressure	1748.88 Pa	Achieved IT > 201	62.6426 Pa	1743.44 Pa
GG Maximum Static Pressure 1	105407 Pa	Achieved IT > 201	487.114 Pa	105407 Pa
SG Average Shear Stress 1	3.31289 Pa	Achieved IT > 228	0.0220023 F	3.30921 Pa

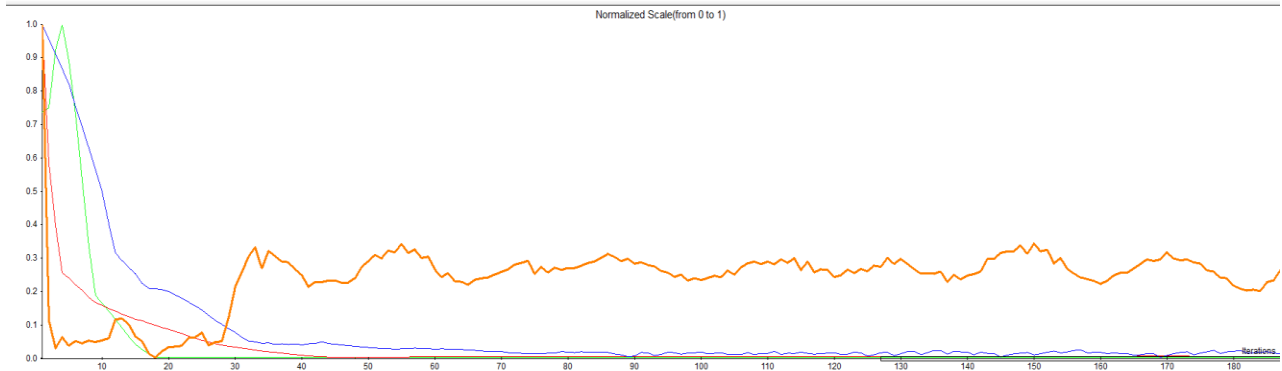


Figure 43: Goals iteration graph

4.2 Prototype Testing

The experimental setup is documented before running specific tests. Subsequent tests are tabulated in following orders: waterproofing test to ensure no leakage, buoyancy test to determine depth stability, manoeuvrability test to evaluate ROV motion, thruster performance test, and power consumption test.

Table 14: *General Setup*

General Test Information		Conditions
Test Location		Outdoor swimming pool
Water Depth		1.8 metres
Environmental Conditions		Clear water, no significant turbulence
Equipment Used		ROV prototype, Stopwatch, Measuring Tape, Buoyancy Line, Camera
Test Setup		Test 1 and 2 in still water Test 3 in slight current from water fountain
Test Duration		Test 1 – 5 minutes Test 2 and 3 – 12 minutes
Test Frequency		Test 1 – 0.5 Hz Test 2 – 1.2 Hz Test 3 – 1.5 Hz

Table 15: *Waterproofing Test*

Type	Leakage Detection (Y/N)?	Leakage Location	Remark
Pre-submersion Check	N	N/A	No gap, no bubbles
Post-submersion (empty enclosure)	Y	Near cable gland joint	Additional sealant applied
Post-submersion (with electronics)	N	N/A	Seal confirmed

Table 16: *Buoyancy Test*

Test No.	Buoyancy Condition	Stability	Remark
1	Negative	Unstable, gradual sink	Not enough thrust, adjust ballast
2	Neutral	Stable	No major vertical shift, smooth motion
3	Slightly Negative	Slightly unstable	High speed increases forward thrust but also turbulence

Table 17: Maneuverability Test

Test No.	Start Position (X, Y, Depth)	End Position (X, Y, Depth)	Time taken (s)	Speed (cm/s)	Observation
1	(0,0,1.5)	(10,0,1.71)	277	3.6	Steady speed, slight delay in response
2	(0,0,1.5)	(10,0,1.5)	131	7.6	Smooth motion, steady speed
3	(100,0,1.5)	(0,0,1,1.57)	185	5.4	Slightly reduced speed due to current
Expected (5 Hz)	(0,0,1.5)	(10,0,1.5)	83	12	Practical range with drag limitation

Table 18: Thruster Performance Test

Test No.	Observed Thrust	Observed Efficiency	Remark
1	Minimal movement	Good balance	Sufficient thrust but less than 0.5 Hz is not recommended.
2	Stable propulsion	Optimal setting	Best forward movement in stable conditions, no instability observed.
3	Rapid motion, quite unstable	Slight turbulence	Some vibrations noted.

Table 19: Power Consumption Test

Test No.	Battery Voltage (Before, V)	Battery Voltage (After, V)	Current Draw (A)	Servo Response Time (s)	Remark
1	6.48	6.4	0.7	0.12	Normal discharge rate
2	6.4	6.27	1	0.16	Slight increase in draw during turning
3	6.31	6.1	1.2	0.15	Under full thruster operation, more load

The final testing results demonstrate the successful implementation of bio-inspired thruster to ROVs. Speed increases with higher flapping frequencies. This indicates that the propulsion system effectively converts oscillatory motion into forward thrust. Even with 1.2 Hz frequency, the ROV moved at expected motion. In extrapolated expectation at 5 Hz, the predicted speed is 12 cm/s. This surpassed many existing small ROV models in its category. The battery voltage-drop also remained within expected values. With careful fine-tuning with buoyancy, particularly in dynamic current conditions, consistent and efficient performance can be achieved. Moreover, the input values are not even near the maximum limits, thus better results can be expected while operating at full potential.

4.3 Integration to ROV Framework

Current thruster design can be integrated or modified for broader ROV applications by evaluating these aspects.

Structural Adaptation – Existing small-scale ROVs typically use rigid-frame designs with conventional thrusters mounted at fixed positions. For bio-inspired design, it requires lateral attachment points for fins. Given that many small-scale ROVs feature open-frame designs, the current prototype's attachment method can be modified to fit within standard configurations.

Power and Control System Compatibility – Most small-scale ROVs rely on brushless DC motors, powered by battery systems ranging from 12V to 24V. The tested bio-inspired thruster operates within a 6V–6.5V range with a current draw peaking at 1.2A. This makes it compatible with existing low-power control architectures. Additionally, ROVs using microcontrollers such as Arduino, can accommodate the thruster system with minimal modifications. The use of PWM signals for servo control aligns with standard ROV electronics, ensuring seamless integration.

Hydrodynamic Performance – Bio-inspired thruster demonstrated a speed of 7.6 cm/s at 1.2 Hz, offers a natural undulating movement. This potentially reduces water disturbance and drag effects. Compared to small ROVs with speeds ranging from 0.138 m/s to 0.31 m/s, the current prototype's motion is competitive at its tested frequencies. With further frequency optimization, it has the potential to meet or exceed conventional thruster speeds while maintaining energy efficiency.

5. Conclusion

This project successfully designed, developed, and tested a bio-inspired thruster system for small-scale ROV applications. It achieves the objectives of the project through simulations and experiments. The prototype demonstrated stable forward motion, effective thrust generation, and compatibility with existing ROV frameworks. This validates the feasibility of bio-inspired propulsion in underwater robotics.

Compared to conventional propeller-driven ROVs, the bio-inspired thruster offers advantages in energy efficiency, reduced turbulence and noise pollution. It is also adaptable to confined environments. Its ability to integrate seamlessly into existing ROV frameworks—without significant modifications to power and control systems—demonstrates its viability for applications requiring precise and low-disturbance manoeuvrability.

Future developments should focus on refining frequency control, optimizing fin design, and exploring multi-thruster configurations to further enhance performance. The findings contribute to the advancement of bio-mimetic underwater robotics, paving the way for more efficient and versatile ROV systems.

6. Recommendation

After successful implementation of the design, several innovations are recommended for further improvement of maneuverability, precision, and control in real-world applications.

1. Integration of vertical fin tail for depth and directional control

To enable more effective vertical adjustments, a tail system is added at the rear end of the ROV. This would function using the same servo and fin mechanism as the lateral fins. This allows controlled upward and downward motion without relying solely on ballast adjustments.

2. Increased Fin Count for Improved Precision

More control surfaces would provide the ability to execute precise turns and maintain steady motion in challenging underwater conditions. Moreover, by programming all fins to move in unison; either all tilting downward for ascent or upward for descent, the ROV could achieve controlled vertical motion without additional hardware.

3. Increased Advanced Control System for Real-Time Pilot Operation

By integrating a more advanced controller interface, operators could manually adjust the frequency and motion of the fins dynamically from above. This enables better responsiveness and adaptability to mission requirements. This would enhance usability and make the bio-inspired thruster system more practical for field applications.

4. Development of a Surface Support Vehicle

To improve deployment and mission efficiency, integrating the ROV with a surface support vehicle could be beneficial. This small surface vessel would serve as a control hub, sending commands to the ROV, managing depth settings, and collecting real-time data from onboard sensors. By maintaining a stable position at the surface, it could lower the ROV to a desired depth before releasing control for horizontal movement.

References

- Abrar, M. M., & Islam, R. (2020, December). Design and development of a biologically inspired robotic cat for research and education. In *2020 30th International Conference on Computer Theory and Applications (ICCTA)* (pp. 82-87). IEEE.
<http://dx.doi.org/10.1109/ICCTA52020.2020.9477678>
- Aguirre-Castro, O. A., Inzunza-González, E., García-Guerrero, E. E., Tlelo-Cuautle, E., LópezBonilla, O. R., Olguín-Tiznado, J. E., & Cárdenas-Valdez, J. R. (2019). Design and construction of an ROV for underwater exploration. *Sensors*, 19(24), 5387.
<https://doi.org/10.3390/s19245387>
- Akmal, M., Yusoff, M., & Arshad. (2012). Active fault tolerant control of a remotely operated vehicle propulsion system. *Procedia Engineering*, 41, 622–628.
<https://doi.org/10.1016/j.proeng.2012.07.221>
- Azis, F., Aras, M., Rashid, M., Othman, M., & Abdullah, S. (2012). Problem identification for underwater Remotely Operated vehicle (ROV): a case study. *Procedia Engineering*, 41, 554–560. <https://doi.org/10.1016/j.proeng.2012.07.211>
- Bianchi, G., Cinquemani, S., & Resta, F. (2021). Bio-inspired design of an underwater robot exploiting fin undulation propulsion. *Applied Sciences*, 11(6), 2556.
<https://doi.org/10.3390/app11062556>
- Binugroho, E. H., Dewanto, R. S., & Pramadihanto, D. (2018, October). erov: Preliminary design of 5 dof rov using 6 thrusters configuration. In *2018 International Electronics Symposium on Engineering Technology and Applications (IES-ETA)* (pp. 281-287). IEEE. <https://doi.org/10.1109/ELECSYM.2018.8615595>

Christ, R. D., & Wernli Sr, R. L. (2007). *The ROV manual: a user guide for observation class remotely operated vehicles*. Elsevier.

Costa, D., Palmieri, G., Palpacelli, M. C., Panebianco, L., & Scaradozzi, D. (2017, September). Design of a bio-inspired autonomous underwater robot. *Journal of Intelligent & Robotic Systems*, 91, 181-192. <https://doi.org/10.1007/s10846-017-0678-3>

Costa, D., Scoccia, C., Palpacelli, M., Callegari, M., & Scaradozzi, D. (2022). Design of a Labriform-Steering Underwater Robot Using a Multiphysics Simulation Environment. *Robotics*, 11(1), 11. <https://doi.org/10.3390/robotics11010011>

DeWijs, B. (2000). AUV/ROV propulsion thrusters. In *OCEANS 2000 MTS/IEEE Conference and Exhibition* (pp. 173–175). IEEE. <https://doi.org/10.1109/OCEANS.2000.881811>

Fotland, K. (2018). *Analysis of ROV thrusters and small marine propellers at specific rotational speeds* (Master's thesis, University of Stavanger, Norway). [http://hdl.handle.net/11250/2562138\](http://hdl.handle.net/11250/2562138)

Gomes, R. M., Martins, A., Sousa, A., Sousa, J. B., Fraga, S. L., & Pereira, F. L. (2005, June). A new ROV design: issues on low drag and mechanical symmetry. In *Europe Oceans 2005* (Vol. 2, pp. 957-962). IEEE. <https://doi.org/10.1109/OCEANSE.2005.1513186>

Gucer, Ç. A., Acar, O., Kantarcioğlu, B., Ulu, C. (2020). THRUSTER DESIGN FOR UNMANNED UNDERWATER VEHICLES. *Selçuk-Teknik Dergisi*, 19(4), 196–208. <http://sutod.selcuk.edu.tr/sutod/article/view/528/723>

Hsieh, M. F., Chen, J. H., Yeh, Y. H., Lee, C. L., Chen, P. H., Hsu, Y. C., & Chen, Y. H. (2007, November). Integrated design and realization of a hubless rim-driven thruster. In *IECON 2007-33rd Annual Conference of the IEEE Industrial Electronics Society* (pp. 3033-3038). IEEE. <https://doi.org/10.1109/IECON.2007.4460298>

Khojasteh, D., & Kamali, R. (2017). Design and dynamic study of a ROV with application to oil and gas industries of Persian Gulf. *Ocean Engineering*, 136, 18–30. <http://dx.doi.org/10.1016/j.oceaneng.2017.03.014>

Kim, T., Kim, J., & Yu, S. C. (2024). Development of Bioinspired Multimodal Underwater Robot “HERO-BLUE” for Walking, Swimming, and Crawling. *IEEE Transactions on Robotics*. <https://doi.org/10.1109/TRO.2024.3353040>

Kökçan, Y. E., & Tamer, Y. (2020). Effect of o-MMT content on properties of Poly (vinyl chloride)/Poly (acrylonitrile styrene acrylate) blends. *Journal of the Turkish Chemical Society Section A: Chemistry*, 7(3), 635-648. <https://doi.org/10.18596/jotcsa.635095>

Liu, Z., & Li, D. (2024). Engineering of a Bio-Inspired Tiltable Oscillating Fin Submersible Thruster. *Robotics*, 13(10), 154. <https://doi.org/10.3390/robotics13100154>

Low, K. H. (2009). Modelling and parametric study of modular undulating fin rays for fish robots. *Mechanism and Machine Theory*, 44(3), 615-632. <https://doi.org/10.1016/j.mechmachtheory.2008.11.009>

Maritim Karriere. (n.d.). *Professions: FU-operatør – control the underwater robot.* <https://maritimkarriere.no/yrker/fu-operator>

Mateos, L. A. (2020). Particle robots A new specie of hybrid bio-inspired robotics. *arXiv preprint arXiv:2003.08289*. <https://doi.org/10.48550/arXiv.2003.08289>

Niikura, A., Nabae, H., Endo, G., Gunji, M., Mori, K., Niiyama, R., & Suzumori, K. (2022). Giraffe Neck Robot: First Step Toward a Powerful and Flexible Robot Prototyping Based on Giraffe Anatomy. *IEEE Robotics and Automation Letters*, 7(2), 3539-3546. <http://dx.doi.org/10.1109/LRA.2022.3146611>

Rosid, N. H., Moelyadi, M. A., Budiyono, A., Hafizh, A., & Putra, W. (2018). Product Redesign based on Reverse Engineering and Hydrodynamic Performance Optimization Using Evolutionary Algorithm of Underwater Thruster. In *ICIUS 2018, Jeju, South Korea* [Conference-proceeding].

Salem, K. M., Rady, M., Aly, H., & Elshimy, H. (2023). Design and implementation of a Six-Degrees-of-Freedom Underwater remotely operated vehicle. *Applied Sciences*, 13(12), 6870. <https://doi.org/10.3390/app13126870>

Shang, L., Wang, S., Tan, M., & Cheng, L. (2012). Swimming locomotion modeling for biomimetic underwater vehicle with two undulating long-fins. *Robotica*, 30(6), 913-923. <https://doi.org/10.1017/S0263574711001159>

Scaradozzi, D., Palmieri, G., Costa, D., Zingaretti, S., Panebianco, L., Ciuccoli, N., Pinelli, A., & Callegari, M. (2017). UNIVPM BRAVe: A hybrid propulsion underwater research vehicle. *International Journal of Automation Technology*, 11(3), 404–414. <https://doi.org/10.20965/ijat.2017.p0404>

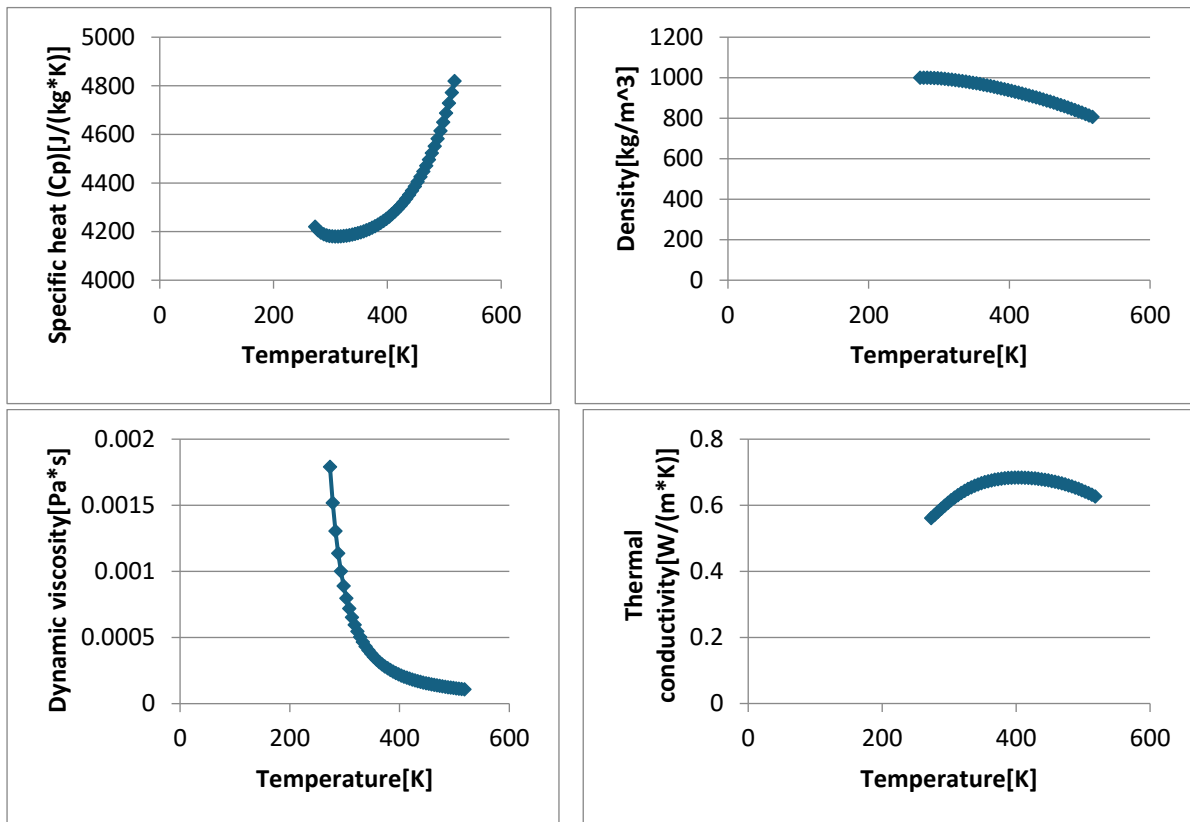
Toda, Y., Suzuki, T., Uto, S., & Tanaka, N. (2004). Fundamental study of a fishlike body with two undulating side-fins. In *Bio-mechanisms of Swimming and Flying* (pp. 93-110). Springer Japan. http://dx.doi.org/10.1007/978-4-431-53951-3_8

Zhang, Y., Wang, S., Wang, X., & Geng, Y. (2018, June). Design and control of bionic manta ray robot with flexible pectoral fin. In *2018 IEEE 14th International Conference on Control and Automation (ICCA)* (pp. 1034-1039). IEEE. <https://doi.org/10.1109/ICCA.2018.8444283>

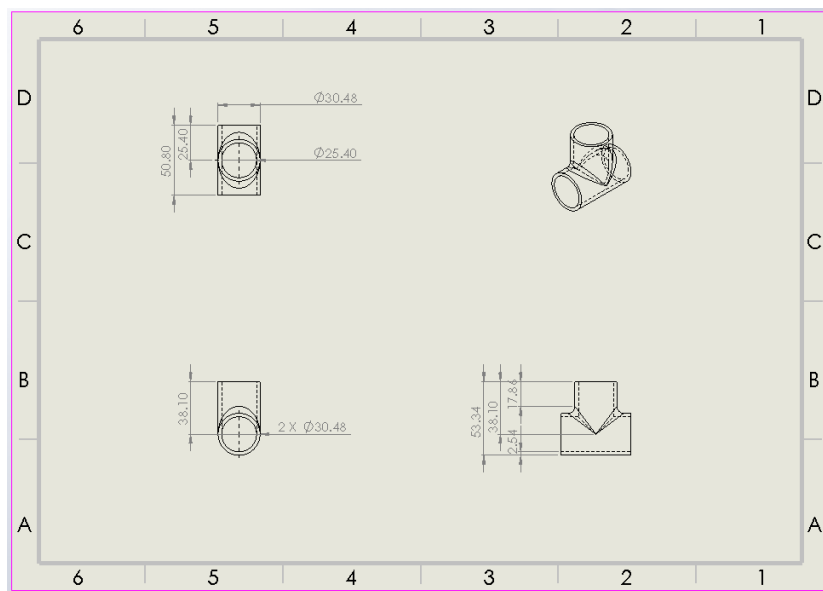
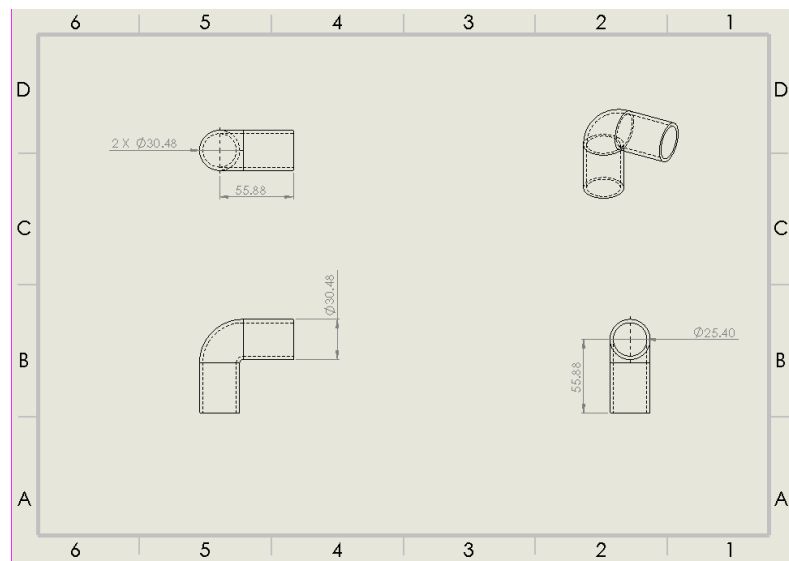
Zhou, B., & Zhao, M. (2020). Numerical simulation of thruster-thruster interaction for ROV with vector layout propulsion system. *Ocean Engineering*, 210, 107542. <https://doi.org/10.1016/j.oceaneng.2020.107542>

Zhu, X., & Li, W. (2021, August). Research on Dynamic Compression Testing of Silicone Rubber under Different Temperatures. In *Journal of Physics: Conference Series* (Vol. 2002, No. 1, p. 012047). IOP Publishing. <https://doi.org/10.1088/1742-6596/2002/1/012047>

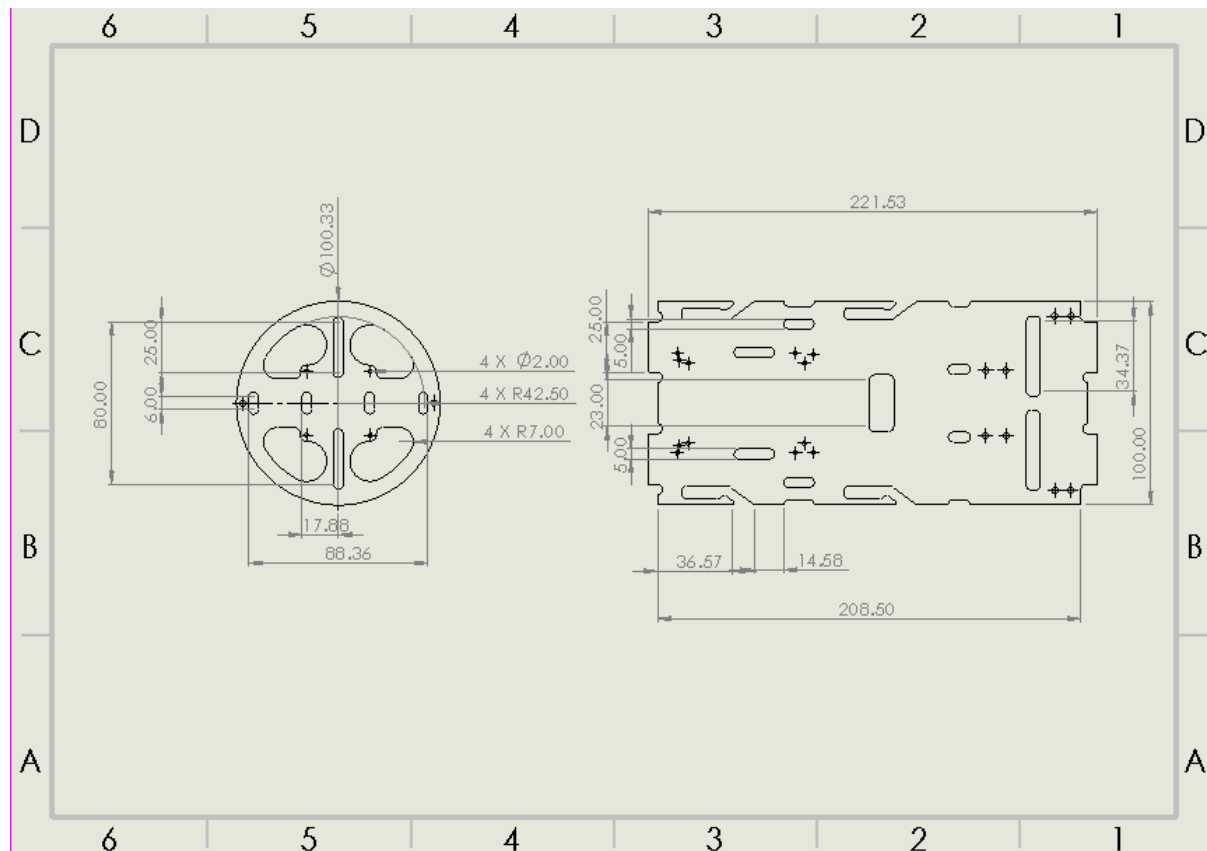
Appendices



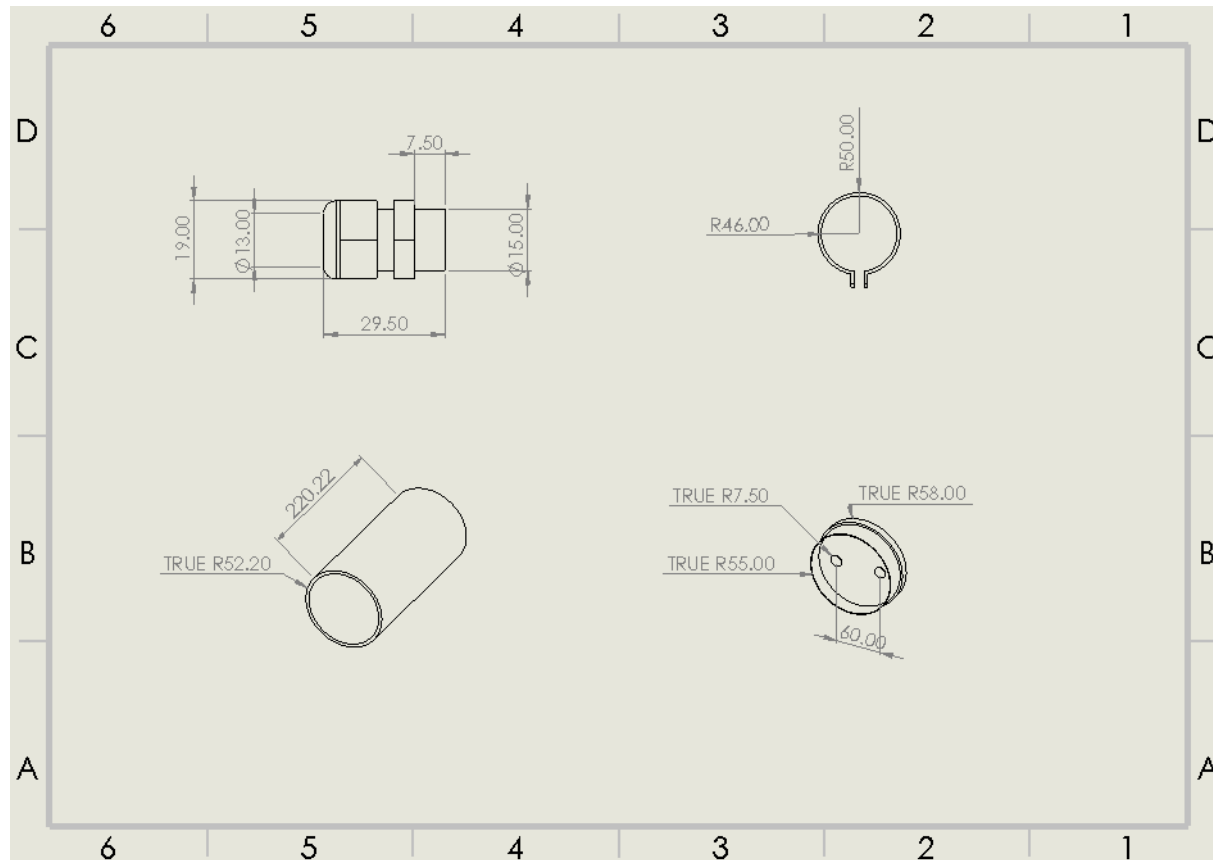
Appendix A – Path: Liquids Pre-Defined (CFD Analysis)



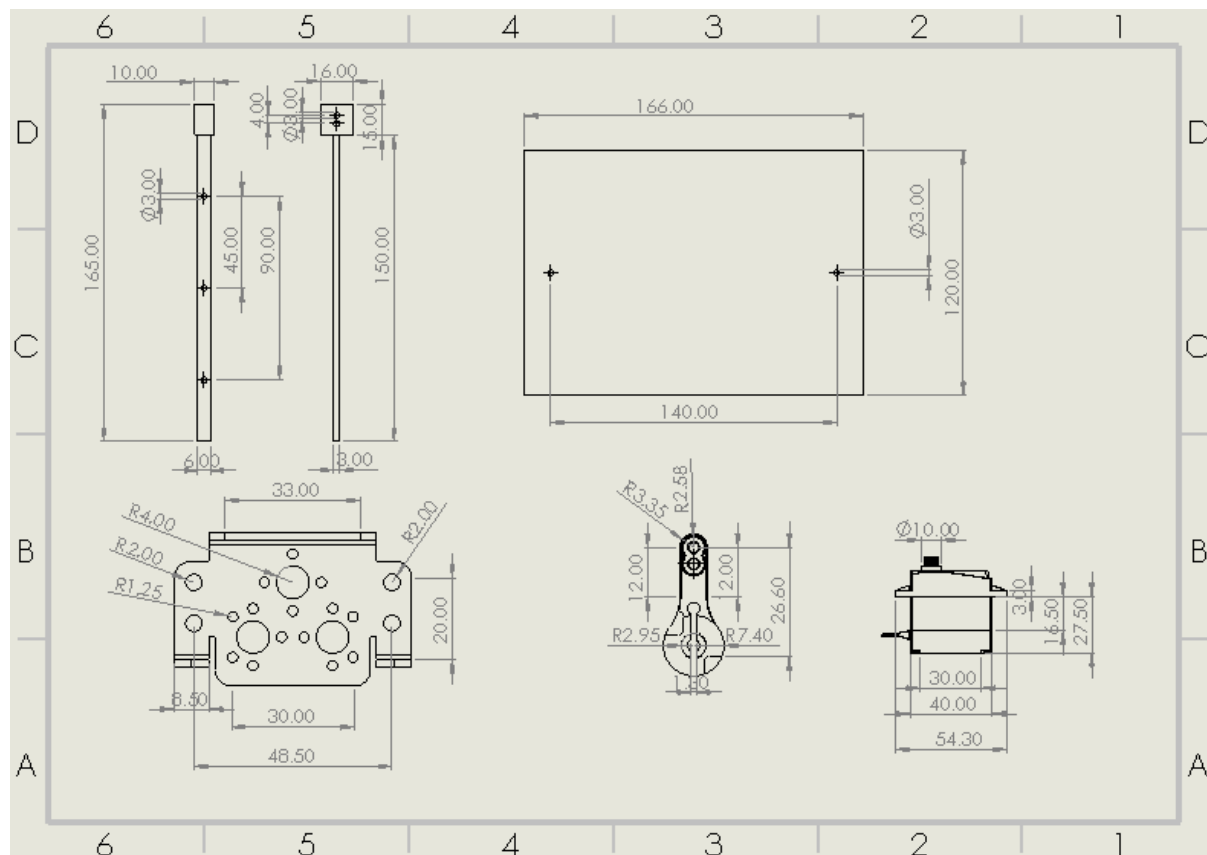
Appendix B – Pipe Joints Dimensions



Appendix C – Electronics Tray Dimensions



Appendix D – Enclosure Dimensions



Appendix E – Fin Assembly Dimensions

		Complexity Cc (blank = not feasible)							
		Process							
		Impact Ext.	Sand Cast	Die Cast	Forge	Press	Machine	Powder Met	Plastic Mould
Complexity	A1	1	1	1	1		1	1	1
	A2	1	1.2	1.1	2.1		1.2	2.1	1.1
	A3	3	1.3	1.3	2.3		2.9	2.3	1.3
	A4		1.8	2	2.6		5.3	2.6	2
	A5		3.2	3.8	3		6.1	4	3.8
	B1	2	1.1	1	1		1	1	1
	B2	3	1.2	2.2	2.2		1.3	1.3	1.3
	B3	5	1.4	2.2	2.2		2.6	1.7	1.8
	B4		1.8	2.3	2.3		2.6	1.7	1.8
	B5		2.6	2.7	2.7		2.8	3.5	3
	C1	1.5	2.1	2.1	1	1	1	1	1
	C2	3	2.3	2.2	1.2	1.2	1.4	1	1.2
	C3	3.5	2.8	2.3	1.6	1.5	3.1	1.4	1.8
	C4		3.7	2.5	2.5	2.2	5.4	2.4	2.9
	C5		5	3.6	3.4	2.5	6.5	4	3.6

Appendix F – Complexity DFM

		Material Suitability Cmp (blank = unfeasible)						
MATERIAL	Impact Ext	PROCESS						
		Sand Cast	Die Cast	Forge	Press	Machine	Powder Met	Plastic Mould
MATERIAL	Cast Iron	1				1.2	1.6	
	Low-C Steel	1.3	1.2	1	1.2	1.4	1.2	
	Alloy Steel	2	1.3	2	1.5	2.5	1.1	
	Stainless Steel	2	1.5	2	1.5	4	1.1	
	Copper Alloys	1	1	1	1	1.1	1	
	Aluminum Alloys	1	1	1.5	1	1	1	
	Zinc Alloys	1	1	1.2	1	1.1	1	
	Thermoplastics (nylons, acrylics, etc.)					1.1		1
	Thermosets (epoxies, phenolics, etc.)					1.2		1
	Elastomers (rubbers)					1.1		1.5

Appendix G – Suitability DFM

		Limiting Section Cs (millimetres) (blank = not feasible)							
		Impact Ext.	Sand Cast	Die Cast	Forge	Press	Machine	Powder Net	Plastic Mould
Min Section (mm)	<= 0.4	1				1	1.6		2
	>0.4 - 0.6	1		1.5		1	1.4		1.2
	>0.6 - 1.0	1		1	1.5	1	1	1.2	1
	>1.0 - 3.0	1	2	1	1	1	1	1	1
	>3.0 - 5.0	1	1	1	1	1.2	1	1	1
	>5.0	1	1	1	1	1.7	1	1	1

Appendix H – Section DFM

		Tolerance Ct (Based on number of planes on which critical tolerances occur)																							
		PROCESS																							
		Impact Ext			Sand Cast			Die Cast			Powder Met			Forge			Press Working			Plastic Mould			Machine		
		1	2	3+	1	2	3+	1	2	3+	1	2	3+	1	2	3+	1	2	3+	1	2	3+	1	2	3+
TOLERANCE (mm)	<- 0.004	3.7	5.3	6.1	4.6	5.6	6.8	5.1	6.1	7	3.1	4.6	5.4	4.3	5.6	6.6	4.6	5.4	6.5	4.8	6.3	7.1	3.7	5.3	
	>0.004-0.01	2.8	3.1	4.3	3.5	3.8	4.9	3.5	4.2	5	1.4	1.7	2.1	3.2	3.5	4.6	3.2	3.8	4.5	3.6	3.9	5.2	2.8	3.1	4.3
	>0.01-0.03	1.9	2.4	2.6	2.8	3	3.2	2.8	3	3.6	1	1.1	1.4	2.6	2.8	3	2.6	2.8	3.2	2.9	3.4	3.4	2.2	2.4	2.6
	>0.03-0.05	1.1	1.5	1.9	2.4	2.5	2.8	2.8	2.5	2.8	1	1	1	2.3	2.4	2.5	2.2	2.4	2.5	1.9	2.1	2.3	1.2	1.4	1.6
	>0.05-0.08	1	1	1	2.2	2.4	2.5	1.5	2	2.4	1	1	1	2.2	2.3	2.4	1	1.4	1.6	1	1	1	1.1	1.2	1.4
	>0.08-0.15	1	1	1	2	2.2	2.4	1	1.4	2	1	1	1	1.9	2.2	2.3	1	1	1	1	1	1	1	1.1	1.2
	>0.15-0.3	1	1	1	1.9	2	2.2	1	1	1	1	1	1	1.8	1.9	2.2	1	1	1	1	1	1	1	1	1.1
	>0.3	1	1	1	1.5	1.7	1.9	1	1	1	1	1	1	1.4	1.6	1.8	1	1	1	1	1	1	1	1	1

Appendix I – Tolerance DFM

		Surface Finish Cf (Based on number of planes on which critical surface finishes occur)																							
		PROCESS																							
		Impact Ext			Sand Cast			Die Cast			Powder Met			Forge			Press Working			Plastic Mould			Machine		
		1	2	3+	1	2	3+	1	2	3+	1	2	3+	1	2	3+	1	2	3+	1	2	3+	1	2	3+
SURFACE FINISH (micrometre)	super fine ground	<=0.4	4.3	5.1	6.3	4.9	5.6	6.6	4.3	5.1	6.3	4.3	5.1	6.3	4.9	5.6	6.6	4.4	5.3	6.8	1.2	1.2	1.2	4.1	4.8
	fine ground	>0.4-0.6	2	2.5	2.9	3.9	4.2	4.6	1.2	1.5	1.7	2	2.5	2.9	3.2	3.4	3.8	1.3	1.5	1.8	1	1	1	1.2	1.5
	medium ground	>0.6-0.8	1.1	1.2	1.4	3	3.2	3.5	1.1	1.2	1.5	1.1	1.2	1.5	2.6	2.8	3	1.1	1.2	1.5	1	1	1	1.1	1.3
	coarse ground	>0.8-1.0	1	1.1	1.2	2.5	2.6	3	1	1.1	1.3	1	1.1	1.3	2.3	2.4	2.6	1	1	1.2	1	1	1	1	1.3
	semi fine	>1.0-3.0	1	1	1	2.3	2.4	2.6	1	1	1	1	1	1	1.9	2	2.2	1	1	1	1	1	1	1	1
	medium fine	>3.0-5.0	1	1	1	2	2.1	2.3	1	1	1	1	1	1	1.4	1.5	1.7	1	1	1	1	1	1	1	1
	semi rough	>5.0-10.0	1	1	1	1.9	2	2.1	1	1	1	1	1	1	1.1	1.3	1	1	1	1	1	1	1	1	1
	very rough	>10.0	1	1	1	1	1.1	1.3	1	1	1	1	1	1	1	1	1	1	1	1	1	1	1	1	1

Appendix J – Surface Finish DFM

		Basic Processing Cost/Quantity Pcs								
		PROCESS								
		Impact Ext	Sand Cast	Die Cast	Forge	Press	Auto M/C	Manual M/C	Power Met	Plastic Mould
Per Annum Quantity	10	20000	513	10000	15000	8000	5000	505	50000	10000
	50	4000	113	2000	3000	1600	1000	105	10000	3000
	100	2000	63	1000	1500	800	500	55	5000	1000
	200	1000	38	500	750	400	250	30	2500	500
	400	500	26	250	376	200	126	18	1250	250
	600	330	21	168	251	134	85	14	836	167
	800	250	19	126	189	100	64	11	628	126
	1000	200	18	100	151	80	51	10	500	100
	2000	100	16	51	76	40	26	7.7	253	51
	4000	50	14.3	26	39	20	14	6.5	128	26
	6000	35	13.8	17	26	14	9.6	6	86	17
	8000	26	13.6	13	20	10	7.5	5.8	66	13
	10000	21	13.5	11	16	8	6.2	5.7	53	11
	20000	11	13.3	5.8	8.7	4.4	3.7	5.46	28	5.8
	30000	7.3	13.2	4.1	6.2	3.1	2.9	5.38	19.7	4.1
	40000	5.6	13.1	3.3	5	2.4	2.47	5.34	15.5	3.3
	50000	4.6	13.1	2.8	4.2	2	2.22	5.31	13	2.8

Appendix K – Ideal Processing DFM

Basic Processing Cost/Quantity P _c (continued)										
		PROCESS								
		Impact Ext	Sand Cast	Die Cast	Forge	Press	Auto M/C	Manual M/C	Power Met	Plastic Mould
Per Annum Quantity	60000	3.9	13.1	2.4	3.7	1.8	2.05	5.29	11.4	2.4
	70000	3.5	13.1	2.2	3.4	1.6	1.93	5.28	10.2	2.2
	80000	3.3	13.1	2	3.1	1.4	1.85	5.27	9.3	2
	90000	2.8	13.1	1.9	2.9	1.3	1.78	5.26	8.6	1.9
	100000	2.6	13.1	1.78	2.7	1.2	1.72	5.26	8.	1.8
	200000	1.61	13	1.28	1.97	0.83	1.47	5.24	5.54	1.3
	400000	1.11	13	1	1.59	0.63	1.35	5.22	4.29	1
	600000	0.94	13	0.95	1.47	0.57	1.3	5.22	3.87	0.95
	800000	0.86	13	0.91	1.47	0.53	1.28	5.21	3.67	0.91
	1000000	0.81	13	0.88	1.37	0.51	1.27	5.21	3.54	0.88
	1500000	0.74	13	0.85	1.32	0.49	1.25	5.21	3.37	0.85
	2000000	0.71	13	0.83	1.3	0.47	1.24	5.21	3.29	0.83
	2500000	0.69	13	0.82	1.28	0.47	1.24	5.21	3.24	0.82
	3000000	0.67	13	0.81	1.27	0.46	1.24	5.21	3.21	0.81

Waste Coefficient W _c (blank = unfeasible)									
		PROCESS							
		Impact Ext	Sand Cast	Die Cast	Forge	Press	Machine	Powder Met	Plastic Mould
Complexity	A1	1	1.1	1	1.1		1.6	1	1
	A2	1	1.1	1.1	1.1		2	1	1.1
	A3	1	1.2	1.1	1.2		2.5	1	1.1
	A4		1.3	1.2	1.2		3	1	1.2
	A5		1.4	1.3	1.3		4	1.2	1.3
	B1	1	1.1	1	1.1		1.7	1	1
	B2	1	1.1	1.1	1.1		2.2	1	1.1
	B3	1	1.2	1.1	1.2		2.8	1	1.1
	B4		1.3	1.2	1.2		4	1	1.1
	B5		1.4	1.3	1.3		6	1.2	1.2
	C1	1	1.1	1.1	1.1	1.2	1.8	1	1
	C2	1	1.2	1.1	1.1	1.2	2.4	1	1.1
	C3	1	1.3	1.1	1.1	1.4	4	1	1.1
	C4		1.4	1.2	1.2	1.5	6	1	1.1
	C5		1.6	1.3	1.3	1.6	8	1.2	1.2

Appendix L – Basic Processing & Waste DFM

Material Cost Selection Cmt	
MATERIAL	C_{mt} (pence/mm³)
Cast Iron	0.00 045
Low Carbon Steel	0.00 039
Alloy Steel	0.00 148
Stainless Steel	0.00 195
Copper Alloy	0.00 245
Aluminum Alloy	0.00 078
Zinc Alloy	0.00 117
Thermoplastics Nylons, acrylics, etc.	0.00 061
Others	0.00 017
Thermosets	0.00 033
Elastomers	0.00 017

Manufacturing Cost Index

The Manufacturing Cost Index, Mi, is given by:

$$Mi = Rc \times Pc + Mc$$

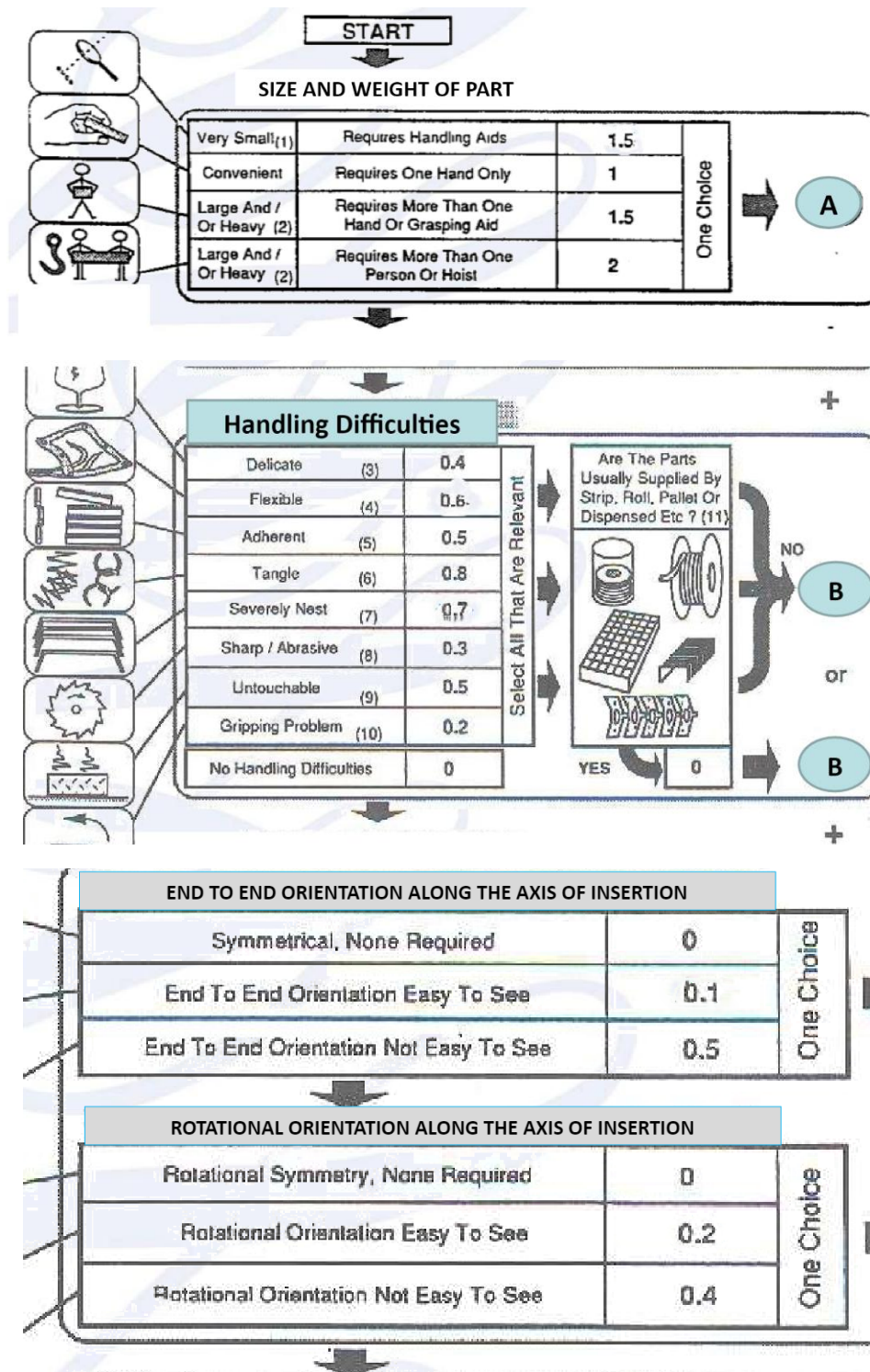
$$Mi = \frac{Rc = \text{Relative Cost}}{\begin{array}{l}Cc = \text{Shape Complexity} \\ Cmp = \text{Material Suitability} \\ Cs = \text{Minimum Section} \\ Ct = \text{Tolerance Requirement} \\ Cf = \text{Surface Requirement}\end{array}} \times \frac{Pc = \text{Ideal Process Cost}}{\begin{array}{l}Pc = \text{Basic Processing Cost} \\ (\text{Ideal Design})\end{array}} + \frac{Mc = \text{Material Cost}}{\begin{array}{l}V = \text{Volume Of Material} \\ Wc = \text{Waste Coefficient} \\ Cmt = \text{Cost Of Material}\end{array}}$$

$$Rc = Cc \times Cmp \times Cs \times Cf \dagger$$

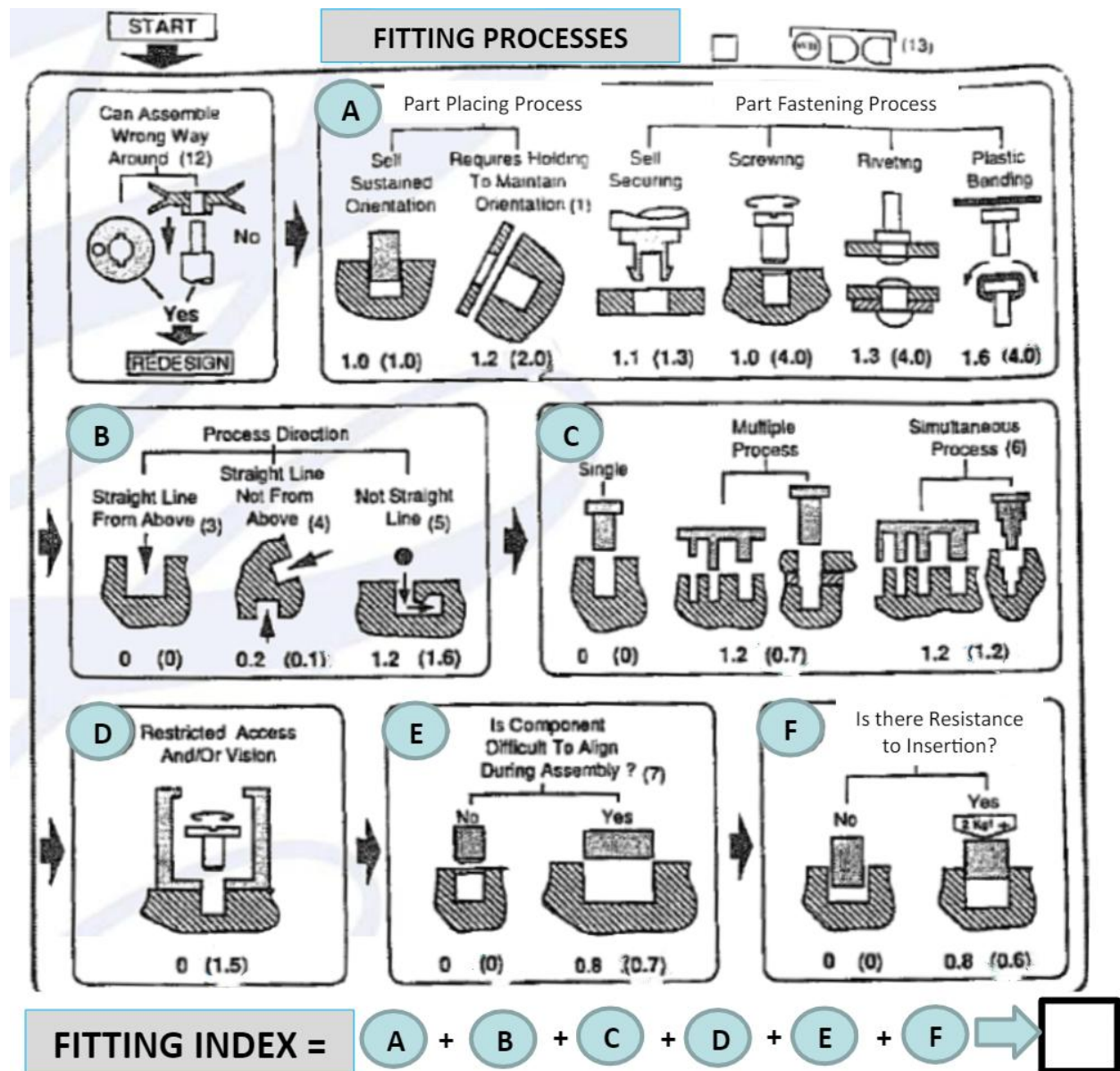
$$Pc \dagger \dagger$$

$$Mc = V \times Cmt \times Wc \dagger \dagger$$

Appendix M – MCI Calculation DFM



Appendix N – Handling Index DFA



Appendix O – Fitting Index DFA